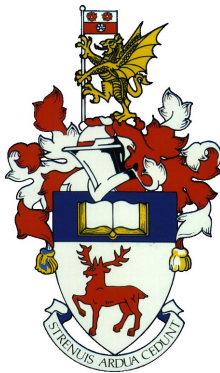


University of Southampton
Faculty of Physical Sciences and Engineering
School of Electronics and Computer Science



Embedded System for Condition Monitoring of Marine Pumps

By

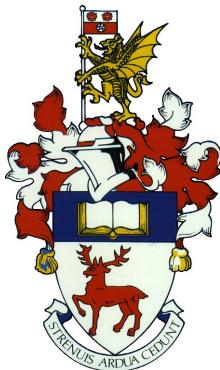
Timothy James Guite

September 6, 2018

Supervisor: Dr Alex Weddell
Second Examiner: Dr Frederic Gardes

A dissertation submitted in partial fulfillment of the degree of
MSc Embedded Systems

University of Southampton
Faculty of Physical Sciences and Engineering
School of Electronics and Computer Science



Embedded System for Condition Monitoring of Marine Pumps

By

Timothy James Guite

September 6, 2018

Supervisor: Dr Alex Weddell
Second Examiner: Dr Frederic Gardes

A dissertation submitted in partial fulfillment of the degree of
MSc Embedded Systems

Abstract

The maritime industry has been slow to adopt the principles of condition monitoring, which supports efficient maintenance decisions across a variety of industries. Small pumps on board ships are often ignored and fixed only after failure. Cheap and effective solutions are required, as commercial condition monitoring systems are too expensive to justify widespread deployment.

The effectiveness of simple signal processing techniques in detecting and diagnosing faults is demonstrated on the Condition Monitoring Laboratory at the national Centre for Advanced Tribology at Southampton (nCATS). An embedded condition monitoring system is broken down into basic modules which are each tested thoroughly. Motor Current Signature Analysis (MCSA) and vibration analysis are combined to provide a robust solution suited to the demands of marine pumps. On-line processing of the time and frequency domain is implemented to take advantage of specialised fault detection methods. An embedded system which performs online processing and fault diagnosis is designed and tested. It is shown to consistently indicate the condition of a motor system as faults are induced and removed. Power consumption of the system is measured, providing a platform from which to integrate developments in low power systems and energy harvesting.

Low cost hardware and simple signal processing techniques are shown to form an effective condition monitoring system. This work leads the way for development of intelligent commercial systems for condition monitoring of marine pumps.

Acknowledgements

I would like to thank the following people and groups for their help in completion of this project:

Dr Alex Weddell, for his help and guidance in this project.

Professor Ling Wang and the design innovation team at Lloyd's Register for forming the industrial partnership that drove this project.

Dr Terry Harvey and Imran Bashir for their practical help in the nCATS laboratory.

The technicians in the ECS Student Laboratory and Mechanical Workshop for being so helpful and engaging, no matter the problems brought to them.

Joyce Lewis, for helping me find the right course.

Statement of Originality

I have read and understood the ECS Academic Integrity information and the University's Academic Integrity Guidance for Students.

I am aware that failure to act in accordance with the Regulations Governing Academic Integrity may lead to the imposition of penalties which, for the most serious cases, may include termination of programme.

I consent to the University copying and distributing any or all of my work in any form and using third parties (who may be based outside the EU/EEA) to verify whether my work contains plagiarised material, and for quality assurance purposes.

I have acknowledged all sources, and identified any content taken from elsewhere.

I have used the KissFFT library under a BSD license, and the pynmea2 library under a MIT license.

I did all the work myself and have not helped anyone else.

The material in this report is genuine, and I have included all my data, code and designs.

I have not submitted any part of this work for another assessment.

My work did not involve human participants, their cells or data, or animals.

Contents

List of Figures	VI
Abbreviations	VIII
1 Introduction	1
2 Background	3
2.1 Maintenance Strategies	3
2.1.1 Corrective and Time-Based Maintenance	3
2.1.2 Condition Based Maintenance	4
2.1.3 Maintenance in the Maritime Industry	5
2.2 Condition Monitoring	6
2.2.1 Signal Processing Techniques	6
2.2.2 Fault Detection and Diagnostics	9
2.2.3 Vibration Analysis	10
2.2.4 Motor Current Signature Analysis	12
2.2.5 Prognostics	16
2.3 Condition Monitoring Systems	16
2.3.1 Existing Market Solutions	17
2.3.2 Embedded Systems	17
3 Fault Detection and Diagnosis with Offline Processing	19
3.1 Condition Monitoring Laboratory	19
3.2 Experimental Methodology	19
3.3 Results	21
3.4 Evaluation	22
4 Modular Development of Embedded System	25
4.1 Online Processing	25
4.2 ADC	27
4.3 Accelerometers	28
4.4 Current Sensors	32
5 Validation of Embedded Systems Approach	35
5.1 Vibration Analysis	35
5.1.1 Sensor Comparison	35
5.1.2 Condition Monitoring	37
5.2 MCSA	40
5.2.1 Phases	40

CONTENTS

5.2.2	Condition Monitoring	40
5.2.3	Speeds	41
5.3	Evaluation	42
6	Embedded System for Online Fault Detection and Diagnosis	44
6.1	System Design	44
6.1.1	Hardware	44
6.1.2	Software	44
6.1.3	Condition Decisions	46
6.1.4	Communication	47
6.2	Long Term Test	49
6.3	Power Consumption	52
7	Conclusion and Future Work	54
7.1	Future Work	54
	Bibliography	56

List of Figures

2.1	Bathtub curve (reproduced from [14])	4
2.2	Maintenance methods (adapted from [8])	5
2.3	Frequency spectrum of a simple signal via Fourier Transform	7
2.4	Hilbert Transform (reproduced from [27])	8
2.5	Viewing a signal which changes in time in multiple domains	9
2.6	Recommended mounting points for vibration transducers, reproduced from [23]	12
2.7	Bearing fault severity chart, reproduced from [25]	13
2.8	Implementation of ANNs with fuzzy logic for classification of water pump condition, reproduced from [39]	13
2.9	Typical elements of a squirrel cage induction motor, reproduced from [40]	14
2.10	Healthy current signal for cage rotor induction motor with 36 slots, 32 bars and 2 pole pairs for a) loaded, slip = 6.4% b) unloaded, slip = 0, reproduced from [42]	15
2.11	Park's Vector for experimental current of three-phase, 4 pole, 50 Hz induction motor, reproduced from [45][46]	16
2.12	Wireless Sensor Node for monitoring and fault detection, reproduced from [33]	18
3.1	CML in nCATS Laboratory - a) Photo, b) Diagram, b) reproduced from [57])	20
3.2	Results from investigation of existing condition monitoring setup	22
3.3	Results from investigation of existing condition monitoring setup with only maximum and standard deviation of the frequency spectrum shown	22
3.4	Results after removing DC frequency component	23
3.5	Averaged frequency spectrum for Bearing 2 of CML with annotations	23
3.6	Comparison of results with ISO bearing fault chart	23
4.1	Modular elements of embedded system for condition monitoring	25
4.2	Processing of frequency spectrum online and in Matlab - a) Time signal, b) Frequency spectrum	26
4.3	Test setup for ADC measurements	27
4.4	Frequency spectrum of signals measured with ADC and processed online compared to model	28
4.5	Test setup for MEMS accelerometers	29
4.6	Banana plug mechanical fixing for MEMS sensors on vibration generator	29
4.7	Comparison of RMS of acceleration and maximum of frequency spectrum for MEMS sensors across frequencies	30

LIST OF FIGURES

4.8	Results of accelerometer tests at 2553 Hz	31
4.9	Test setup for validation of current transducers	32
4.10	Current test at 3A	34
5.1	Mechanical fixing for MEMS sensors on bearing	36
5.2	Comparison of <i>ref</i> and MEMS sensors	36
5.3	Time domain measured by <i>ref</i> and MEMS A sensor for different conditions	38
5.4	Frequency domain measured by <i>ref</i> and MEMS A sensor for different conditions	39
5.5	Comparison of statistics from <i>ref</i> and MEMS A sensors	39
5.6	Comparison of statistics from <i>ref</i> and MEMS A sensors against ISO bearing fault chart	40
5.7	Frequency spectrum of CTs in different conditions	41
5.8	Frequency spectrum of stator current measured by current transducers at various motor speeds (legend shared)	42
6.1	Diagram of embedded CMS setup for test on CML at nCATS	45
6.2	Photo of test setup on the CML at nCATS	45
6.3	CT setup for testing of embedded CMS	45
6.4	Software flow chart for embedded CMS	46
6.5	Charts showing how condition is diagnosed using time domain (bearing fault severity) and frequency domain (fault classification)	47
6.6	Damage on CML	49
6.7	Results from long term test time domain compared to ISO bearing fault standard	50
6.8	Overview of results from long term testing of embedded CMS	51
6.9	Annotated current levels for different system states during reading, processing and transmission of data (signals offset in time for clarity)	53

Abbreviations

CM	Condition Monitoring
CMS	Condition Monitoring System
CBM	Condition-Based Maintenance
TBM	Time-Based Maintenance
PM	Preventative Maintenance
ISO	International Organization for Standardization
BD	Big Data
IoT	Internet of Things
ML	Machine Learning
MEMS	Microelectromechanical Systems
MCSA	Motor Current Signature Analysis
RMS	Root-Mean-Square
std	Standard deviation
DFT	Discrete Fourier Transform
FFT	Fast Fourier Transform
STFT	Short-Time Foutier Transform
WA	Wavelet Analysis
FDD	Fault Detection and Diagnosis
ANN	Artificial Neural Network
FMEA	Failure Modes and Effects Analysis
nCATS	National Centre for Advanced Tribology at Southampton
CML	Condition Monitoring Laboratory
RPM	Revolutions Per Minute
STD	Standard Deviation
DC	Direct Current
AC	Alternating Current
ADC	Analogue-to-Digital Converter
CT	Current Transducer
LPM	Low Power Mode

Chapter 1

Introduction

Maintenance is an essential component of asset management, across industries. Machinery becomes damaged as a result of wear or malfunction and needs repair to continue operating properly [1]. Condition Based Maintenance (CBM) uses information about the health of machines obtained through Condition Monitoring (CM) to make efficient maintenance decisions [2]. CBM has proven to be effective at improving reliability and decreasing operating costs, particularly as systems become more complex and higher standards are required [2][3].

The maritime industry has not implemented CBM widely, and many ships operate without explicit maintenance plans [4]. While there can be many hundreds of rotating machines and pumps on board ships, only large and expensive components such as the main engines are monitored closely [5]. However, increased global competition within ship manufacturing provides a demand for added value and business models which consider lifetime costs of the vessel [6][7]. Similar demands in other industries, combined with work on the Internet of Things (IoT) has improved the feasibility of deploying embedded systems to perform online condition monitoring [8][9]. This has led to interest in low cost embedded systems for condition monitoring of marine pumps.

Lloyd's Register is a maritime classification society and consultancy. They have formed an industrial partnership with the University of Southampton to investigate a range of approaches to CM on ships. Existing commercial solutions were found simply to be too expensive [10]. This project sits within the context of a cohesive system which integrates machine learning, physics-based models and user interfaces to improve the reliability and maintainability of ships.

The aim of this work is to develop an embedded Condition Monitoring System (CMS) which uses CM techniques to diagnose the condition of a machine. The capability of low cost sensors and simple signal processing techniques for fault detection and diagnosis (FDD) will be thoroughly assessed.

Much of the literature focuses on developing complex methods for diagnosing specific faults through offline processing [11]. However, there has been relatively little work on how to effectively deploy this knowledge through embedded systems [12]. As a cost focused industry which does not widely perform monitoring, the maritime industry would benefit greatly from low cost solutions which can provide useful information about machine condition [13].

Chapter 2 of this report is a wide ranging literature review. It explains the

motivation for implementing CBM over more traditional maintenance strategies and explains the methods and systems that are used in the rest of the work.

Chapter 3 examines the capability of simple signal processing techniques to diagnose faults, by offline processing of data collected from the Condition Monitoring Laboratory at Southampton.

Chapter 4 presents and tests the individual modules of the embedded system. The results provide confidence in the accuracy of more complex operations performed by the embedded system.

Chapter 5 compares the condition monitoring capabilities of the embedded system to the results from Chapter 3.

Chapter 6 outlines the design and implementation of an embedded system for online fault detection and diagnosis. The system is tested for its accuracy and performance. Power consumption of the system is also measured.

Chapter 7 concludes the work and highlights important areas for future research.

Chapter 2

Background

2.1 Maintenance Strategies

Maintenance strategies are used by companies and organisations to make maintenance decisions about assets, usually machinery [2]. The aim is to keep machines in a state where they can perform tasks as they are required, to a defined standard [14]. Despite the best efforts of designers, machines will always fatigue due to stresses and loads, and will ultimately fail [2]. Failure can be defined in many ways, from breaching performance parameters to complete breakdown, and is specific to the machine and the environment within which it is operating [2]. Organisations which can make better maintenance decisions will make better use of their resources and therefore be more competitive [2]. Costs associated with maintenance vary, but can be as high as 70% in manufacturing, where machine downtime is directly related to output, and represent a large portion of operating budgets across industries [15]. Although maintenance is often viewed through a lens of trying to minimise necessary costs, it can also be a competitive resource [15]. This is especially true when lifetime costs are considered and appropriate marketing strategies are employed [6].

2.1.1 Corrective and Time-Based Maintenance

Traditionally, maintenance strategies can be categorised as Corrective Maintenance or Preventive Maintenance (PM) [14]. Corrective Maintenance describes returning machinery to a healthy state, following some failure. It is also known as run-to-failure and is the simplest maintenance strategy [14]. Although simple and clear, this strategy often results in a lot of downtime, and can result in upstream failures of associated machinery, worsening the impact and cost of failure [2][3]. It should be noted that while more complex maintenance strategies will be discussed throughout the rest of this project, failures can never be entirely avoided and Corrective Maintenance will always be required to some degree.

Alternatively, PM describes performing maintenance prior to failure [2]. When maintenance activities are carried out on a regular basis - either in calendar time or operating time - this is known as Time-Based Maintenance (TBM) or scheduled maintenance [14][8]. TBM relies on the assumption that failure can be predicted and is a function of time [14][8]. For mechanical parts, this function is often modelled using the “Bathtub Curve” [8] (Fig 2.1). The principle is that the machine can be maintained as it nears the end of its useful life and therefore the risk of failure

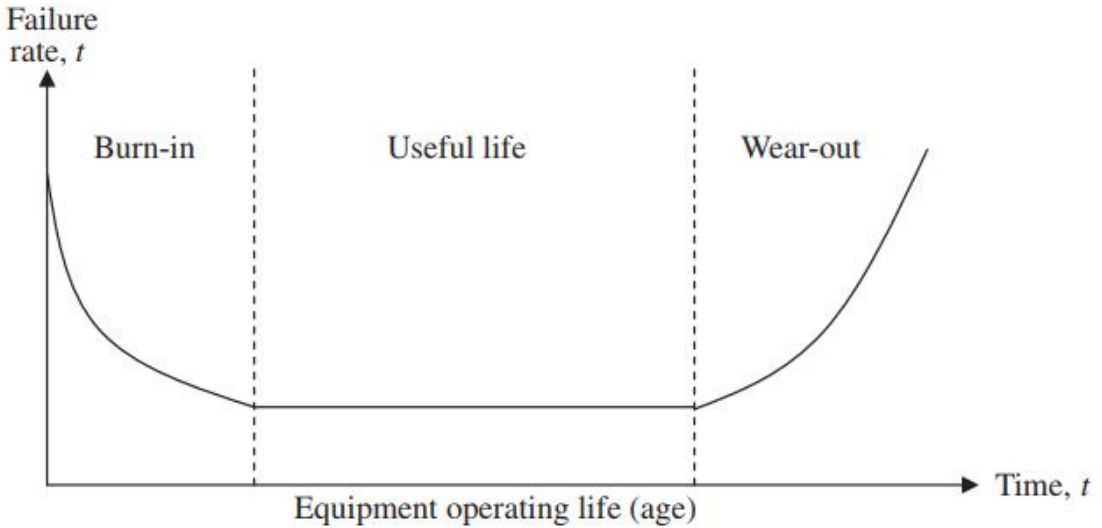


Figure 2.1: Bathtub curve (reproduced from [14])

remains low. The practical issue with TBM is that specific data on failure rates of machinery can be extremely hard to come by, and may not be available at all for specific applications [14]. Therefore, although the “Bathtub Curve” serves as a general model (the ‘burn-in’ period is accounted for by the ISO [16]) it has limited practical applicability and instead the failure rate is often estimated by experienced engineers [14]. While such expertise can be valuable, the organisation will face problems if such an engineer leaves [14]. Assuming a complete set of failure data is available, TBM dictates an optimisation approach to determine the optimal time interval between maintenance activities on a machine. Unfortunately, the complex mathematics associated with this approach can be difficult to interpret and are rarely used in practice [14].

While TBM remains a popular maintenance strategy, it is not the optimal strategy in many cases [2]. There are many opportunities to improve organisational performance and increase profits by implementing more advanced maintenance strategies [4].

2.1.2 Condition Based Maintenance

Condition Based Maintenance (CBM), also known as Reliability Centered Maintenance (RCM), is a maintenance strategy which requires an understanding of the current and future health of machinery to make maintenance decisions [2]. CBM programs have three key stages:

1. Data acquisition
2. Data processing
3. Decision making

The grand aim of CBM is to be able to predict when and how a machine will fail, so that maintenance can be performed just before a failure occurs, increasing the efficiency of maintenance activity [2]. Fig 2.2 demonstrates how CBM finds a balance between many maintenance operations and waiting for total failure. Initially,

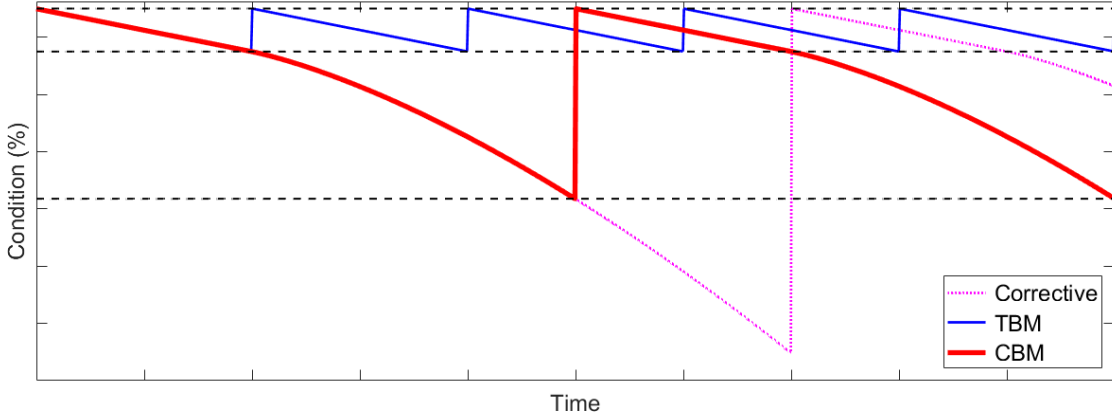


Figure 2.2: Maintenance methods (adapted from [8])

the greatest gains from CBM were made in settings where machines ran for long periods of time with stable loads [3]. Developments in technology have made CBM both more relevant and more practical [2][7]. Systems and machines which require maintenance have become more complex and expensive, while the sensors, processors and algorithms required to implement CBM have become cheaper and more effective [7].

In theory, the exact condition of the machine can be discerned from signals which can be measured externally during operation, such as vibrational and electrical signals [2]. There is extensive literature identifying particular faults in such signals, which will be discussed in more detail in Section 2.2.

As far back as 1978, it was shown that many components and machines fail in a manner that cannot be predicted by age alone [1]. Specifically, an investigation into failure of components on aircraft found that only 11% showed a distinct wear-out zone. This led to a reform towards CBM within the aviation industry [1]. After a significant delay of 5-10 years, the reliability of aircraft improved significantly, and total passenger fatalities have continued to decrease, even as the number of passengers rises; a clear demonstration of the effectiveness of CBM [13].

2.1.3 Maintenance in the Maritime Industry

While CBM has been successfully implemented in many industries, the maritime industry has lagged behind [17]. Costs related to reliability and availability within shipping are estimated at 20 to 30% of operating costs, yet TBM is still the predominant strategy [17][18]. An investigation by Lloyd's Register found that only 17% of classified ships operate with an approved Planned Maintenance System, and even fewer operate CBM [19]. The maritime industry is particularly cost focused and so far, the economic considerations have not justified widespread deployment of CBM [13][17]. Notably, the main engines and other parts of the propulsion system are likely to have a CMS in place. Their enormous cost and importance to the operation of ships does justify the monitoring cost [13]. However, there can be close to 1000 rotating machines on a large ship, which mostly have no regular monitoring, and recording of condition and event data is poor [4].

There have been repeated calls for condition monitoring and CBM to play a

bigger role in the maritime industry [4][20]. Global competition within ship manufacturing may finally provide the necessary impetus for increased uptake of condition monitoring on board ships [6]. By providing lifelong service contracts along with the vessel, ship builders who implement CBM into vessels can compete on quality and lifetime asset cost [6]. The advantage to the ship builders is increased sales and a constant revenue stream. The advantages for the customer are: the likelihood that maintenance costs can be minimised and calculated for by the service contract; service quality is assured across the lifetime of the ship; the customer can focus on their core business. This business model is currently under trial as part of the EU-funded ThroughLife project [6].

Though a novel approach within shipping, other sectors have already developed such models, such as Software-as-a-Service and analytics-as-a-service [7]. These services allow companies to take advantage of BD analytics without necessarily employing experts in-house. Condition monitoring on ships would provide a source of BD which could be powerful as a prognosis tool (Section 2.2.2). Collecting data from a wide range of ships and environments - such as a fleet of vessels - could improve maintainability and influence the design of future vessels [7].

It appears that the maritime industry is ready for CBM and stands to benefit from widespread implementation. However, in a traditionally cost-averse industry, CMSs must have a relatively cheap upfront cost, be accurate, and be introduced alongside business models which offer advantages to ship builders, operators and customers alike [4][7].

2.2 Condition Monitoring

Condition monitoring is the technique which underpins CBM [3]. While it is possible to carefully analyse machines after they have broken and thereby isolate the likely failure mechanism, there are a multitude of techniques available for accurately estimating condition during normal operation. To give a brief list: vibration analysis; motor current signature analysis; oil analysis; thermography; performance analysis; pressure sensing; electrostatic charge sensing; acoustic emissions analysis [2][3][21].

Vibration analysis (Section 2.2.3) is the most widely used method, and Motor Current Signature Analysis (MCSA) (Section 2.2.4) has proven very successful for electric motors. The common factor between them is that data can be collected repeatedly, on-demand, without interfering with operation and can then be analysed with a variety of signal processing techniques [3].

2.2.1 Signal Processing Techniques

Time Domain

The most straightforward method available is looking at the data in the time domain [3]. Simple parameters such as period, peak, mean and standard deviation (std) can be calculated and used to characterise the waveform [22]. More complex measures such as root-mean-square (RMS), skewness, kurtosis have been used to support this characterisation [22]. The RMS of vibration velocity is used by the ISO to give numerical limits for machines [23]. The maximum value and ratio between maximum and RMS can also be indicative of faults related to gearboxes and bearings [24][25].

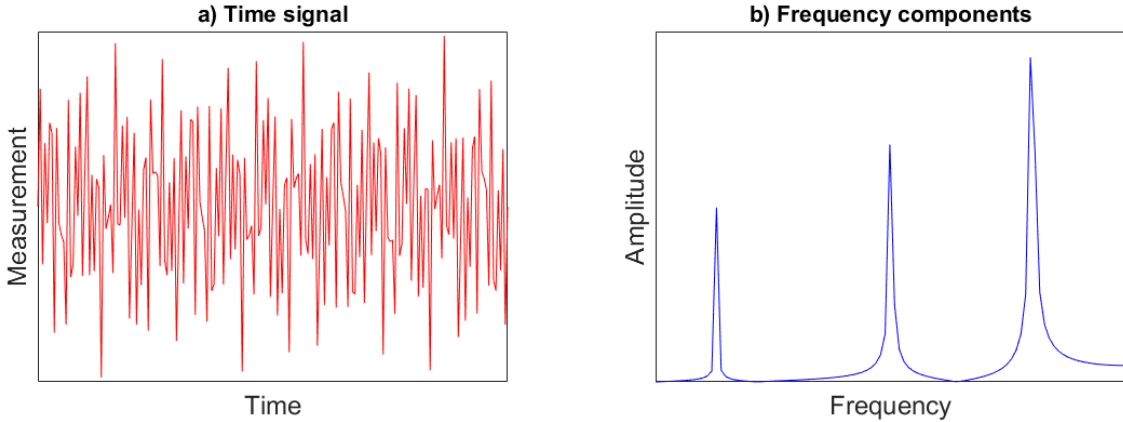


Figure 2.3: Frequency spectrum of a simple signal via Fourier Transform

Many signals contain a large amount of noise that is not related to the machine under inspection. The noise can be treated as a random signal and can therefore be removed to some extent through averaging samples taken at separate times [3]. However, there are many circumstances in which this will not prove effective. Noise may not be random in nature but emanating from other nearby machinery, and changes in operating condition or load will be misrepresented by averaging [3][22]. One solution to these issues is order tracking, which uses information about the position of the machine in its cycle to remove the effects of random speed variations [3]. Often used with rotating machines, where the angle of the shaft is measured by a tachometer or shaft encoder, data is collected at equal intervals of rotation rather than time. Order tracking also allows condition monitoring to take place at a variety of speeds for comparison of resonances. This can then be averaged or processed separately on an angular basis, ensuring that the remaining signal is directly associated with the machine of interest [26].

Information from the time domain is useful for determining an overall picture of machine condition, however it can be difficult to discern differences in the signal and is not particularly effective for specific diagnosis [3].

Frequency Domain

To efficiently extract information, signals are often transformed to the frequency domain. The principle is that any periodic signal is composed of the sum of all possible sinusoids, each of which contribute a certain amount of the signal. Viewing the signal in the frequency domain, the relative input of each frequency can be seen and associated with physical components of the machine [3].

This transformation is well-known as the Fourier Transform. In most modern applications, data is collected at regular intervals (according to the sampling frequency) and therefore the Discrete Fourier Transform (DFT) is used. For time signal f with N samples, frequency bins $F(k)$ are calculated by:

$$F(k) = \sum_{n=0}^{N-1} f[n]e^{-2j\pi kn/N} \quad (2.1)$$

DFT is normally performed using a more computationally efficient method, the Fast-Fourier Transform (FFT), of which there are many variants with specific imple-

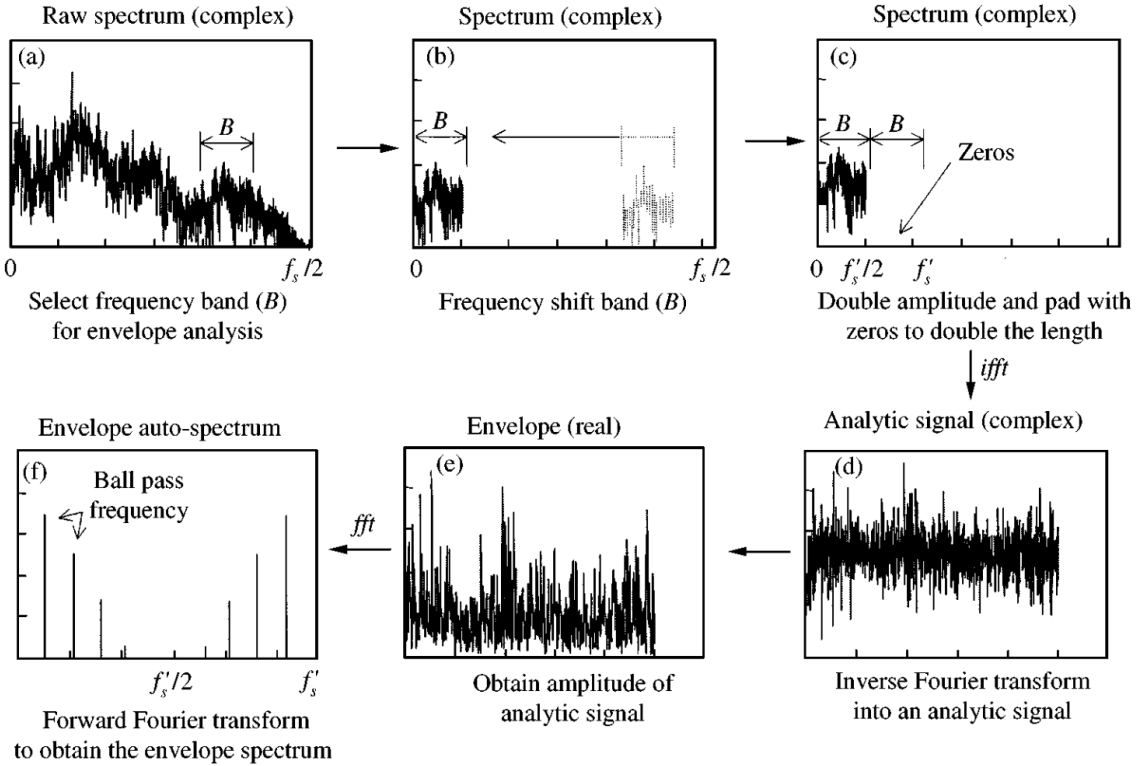


Figure 2.4: Hilbert Transform (reproduced from [27])

mentation advantages [3]. The resolution of the DFT is determined by the sampling rate and the number of samples:

$$f_{res} = f_s/N \quad (2.2)$$

A notable limit on the DFT is the ‘Nyquist Frequency’, which is half the sampling frequency. Any components in the signal above the Nyquist Frequency will cause errors due to aliasing - appearing as other frequencies. Therefore, the sampling frequency should be well above twice the maximum frequency component likely to be measured and in practical applications should be higher still. ISO recommends a frequency range at least 3.5X as high as the largest component of interest [28].

Taking the magnitude of the DFT frequency bins, which store imaginary numbers, gives the frequency spectrum most commonly seen, with a range from 0 Hz to the Nyquist Frequency (Fig 2.3). The shape of this spectrum can be used as a ‘signature’ for certain machine conditions. Starting from a known healthy condition, it is possible to ascertain how the spectrum changes when faults are introduced to the system [3]. In many papers investigating CM, these faults are carefully designed within a laboratory environment, allowing the related components in the frequency spectrum to be identified. The identified components can then be focused on during practical CM.

Noise can also affect the frequency spectrum [3]. Averaging the frequency spectrum over time makes the consistent frequency components clearer, at the cost of diminishing the effect of impulses, which are associated with particular faults and often appear in the higher frequency bands [3]. To remove discrete and random noise around a specific band of frequencies, envelope analysis is performed with the Hilbert Transform (Fig 2.4) [27]. The Hilbert transform has been combined with a

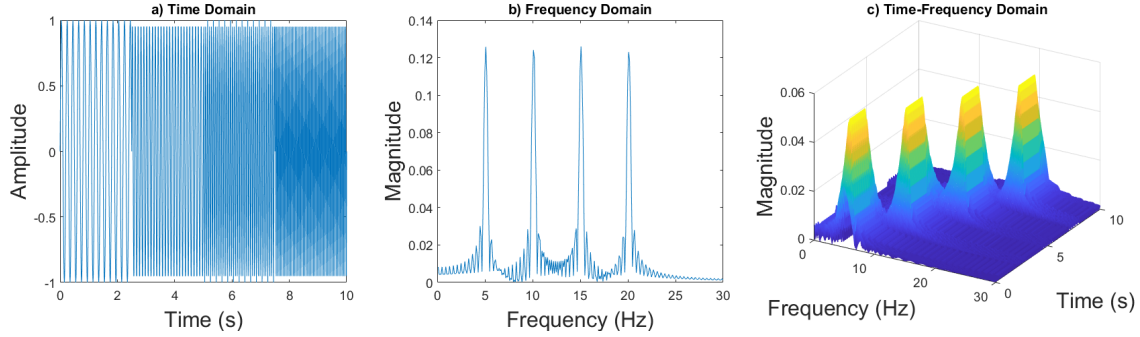


Figure 2.5: Viewing a signal which changes in time in multiple domains

statistical model to identify roller bearing faults in the challenging environment of a helicopter gearbox, although limitations at high frequencies were noted [27].

Literature on detecting and diagnosing faults in the frequency domain is abundant and frequency spectrum analysis continues to be a primary tool for CBM. It provides a clear technique for taking advantage of *a priori* knowledge of the machine, as calculated frequencies can be compared directly to the measured signal [22]. Transforming to the frequency domain is no longer a computational obstacle and provides relevant information for both users and data-driven methods [3]. A large number of condition monitoring systems employ frequency spectrum analysis and specific recommendations are provided by the ISO [28][29].

Time-Frequency Domain

Time-Frequency domain analysis is becoming more common, however the increase in computational complexity is significant [3]. Its purpose is to capture how the frequency spectrum changes with respect to time [22]. This is useful in CM for detecting impulses and other high frequency signals [30]. The challenge in obtaining such information stems from the uncertainty principle, which states that exact information cannot be known about the time and frequency simultaneously [30]. Fig 2.5 demonstrates how a signal with different frequencies at different times can be misinterpreted in the frequency domain but seen much more clearly in the Time-Frequency domain. Short-Time Fourier Transform and Wavelet Analysis are popular Time-Frequency domain transforms [22]. WA in particular has been used for denoising non-stationary signals in the time and frequency domain simultaneously [3]. Evidence of the versatility of WA is provided by its use in denoising and multi-resolution feature extraction of electrocardiogram signals [31].

2.2.2 Fault Detection and Diagnostics

Another important component of CM is the ability to detect and diagnose faults as they occur. While the ISO gives recommendations on how overall vibration levels are related to machine health, being able to diagnose the fault from specific components or statistics provides a significant advantage when making maintenance decisions [23][32]. In an overview of this topic, Dai and Gao [22] highlight three main categories of fault detection and diagnosis:

1. Model-based - Developing state space models and detecting how parameters move away from their expected values

	MCSA	Vib
Easy radial rotor displacement interpretation	✓	✗
Detecting electrical faults	✓	✗
Applicable in rough environments	✓	✗
Cheap implementation	✓	✗
Early stage mechanical fault detection	✗	✓
Distinguish between several bearings in drive train	✗	✓
Knowledge of mean time to failure determination	✗	✓
Favourable noise to signal ration	✗	✓

Table 2.1: MCSA vs Vibration, reproduced from [32]

2. Signal-based - Monitoring how the measured outputs of a system change and correlating with known fault patterns
3. Knowledge-based - Using large amounts of historical data to find patterns and correlations

Each of these approaches relies on having accurate and useful data about the system. The next two sections will provide more in-depth descriptions of the two most successful FDD methods: vibration analysis (2.2.3) and MCSA (2.2.3) [32]. The main advantages of both techniques over the other available options are the relative ease of implementation on a wide range of machines, clear analytical models and data which can be analysed with a variety of methods [22][32]. A brief overview of the differences between the techniques can be seen in Table 2.1. It is clear that not all faults can be detected with MCSA or vibration analysis alone. For example: vibration analysis cannot identify specific faults with the power supply frequency or individual phases; MCSA cannot identify which bearing is faulty along a shaft. While MCSA can provide very specific information on induction motors, varying the load on the motor can provide similar signals to some mechanical faults [32]. Combining the two methods provides coverage of most faults, redundancy of the CMS and allows for specific fault diagnostics [32][33][34].

2.2.3 Vibration Analysis

Vibration analysis takes advantage of the fact that many faults within a rotating machine can be detected and identified from vibration signals produced by the machine. This information can be extracted by measuring displacement, velocity or acceleration [3]. It is generally viewed as the most reliable and widely used condition monitoring method [32].

An important factor in the efficacy of vibration analysis is the mounting location and method [36]. Fig 2.6 shows ISO recommended mounting points for vibration transducers on horizontal pumps. Increasing the number of sensors on a machine helps to build a more complete picture of machine health. Using multiple vibration sensors can provide information about the location of faults, for example indicating which bearing is most likely to be faulty [32]. Additionally, it is essential that the sensors are strongly fixed to their mounting points to accurately measure vibrations

Fault	Frequency	Notes/Causes
Unbalance, misalignment and bent shaft	$k.f_r$	Related and appear strongly at the first few multiples of f_r
Oil whip	$0.6 - 0.95f_r$	Most common fault to appear in the subharmonic range
Bearing inner race (BPFI)	$\frac{k.f_r.n}{2}(1 + \frac{d}{D}\cos\beta)$	Defect on inner race
Bearing outer race (BPFO)	$\frac{k.f_r.n}{2}(1 - \frac{d}{D}\cos\beta)$	Defect on outer race
Ball spin frequency (BSF)	$\frac{k.f_r.d}{2D}(1 - (\frac{d}{D}\cos\beta)^2)$	Defect on rolling element
Bearing cage (FTF)	$\frac{k.f_r}{2}(1 - \frac{d}{D}\cos\beta)$	Defect on cage
Insufficient clearance and expansion of rolling elements	$2 \times BSF$	Bearings can overheat due to improper installation and loading
Lubrication defect	8 kHz octave band	Can cause bearings to heat up
Contamination	8 kHz octave band	Abrasions of bearings and inner surfaces
Looseness of bearing housing	Shocks at f_r	Housing is not correctly sized or excessive loading
Unbalanced power supply voltages	$2f_s \pm \frac{1}{3}f_s$	Can result from loose connections

Table 2.2: Faults which can be detected with vibration analysis - mechanical rotor frequency f_r , integer $k = 1, 2, 3\dots$, number of rolling bearings n , ball diameter d , pitch diameter D , bearing contact angle β , supply frequency for electric motors f_s [3][32][25][35]

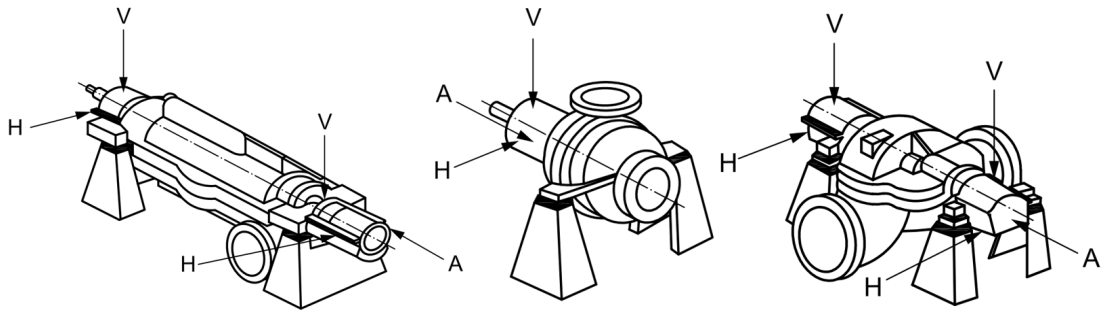


Figure 2.6: Recommended mounting points for vibration transducers, reproduced from [23]

[36]. Screw and stud fittings are the best options as they will perform well in challenging conditions and do not significantly affect the vibration experienced by the sensors [36].

Table 2.2 provides a compilation of faults which can be detected using vibration analysis and the frequencies at which they occur. The frequencies of interest are usually up to 10 kHz [3]. In general, as machines begin to wear and degrade, the overall vibration level increases and can be described by the RMS of vibration data in the time domain [28]. In some instances, measuring how RMS of velocity or acceleration changes over time is the only processing performed. The ISO provide guidance on absolute RMS limits for different categories of machinery [23]. However, RMS is not suitable for detecting short-lived signals associated with gear tooth or bearing failure [24].

As the most common failure cause for rotating machines, bearing faults are widely investigated in the literature [32][35][37]. Envelope analysis has proven effective across a range of experiments for detecting specific bearing faults [3][37][38]. The ISO provide a chart for comparing the severity of bearing faults (Fig 2.7). If the maximum acceleration is much higher than the expected value based on RMS, it is likely a result of impulses which result from faults on the bearing or gearbox. This chart is a simple but effective method for identifying bearing failures.

Work on incorporating machine learning into vibration analysis has shown that simple statistics can be used to classify the condition of the machine [39]. Using only the maximum, RMS and std of the frequency spectrum, an adaptive neuro-fuzzy inference system was trained to differentiate between the healthy condition and two fault conditions (Fig 2.8). Large amounts of data were required for training and testing (100s at 8192 Hz for each condition) and proved very accurate. Notably, training and testing was all performed offline on a computer. This method could be extended to classify other faults.

2.2.4 Motor Current Signature Analysis

For electric motors, MCSA is an extremely powerful tool, and can be used to detect and diagnose faults which are not detectable by vibration alone. However, healthy behaviour, such as changing loads, can appear similar to faults so care must be taken in application [32]. MCSA has a long history of usage which has shown that it is versatile and effective [43].

Induction motors are the most numerous motors for industrial systems, with a

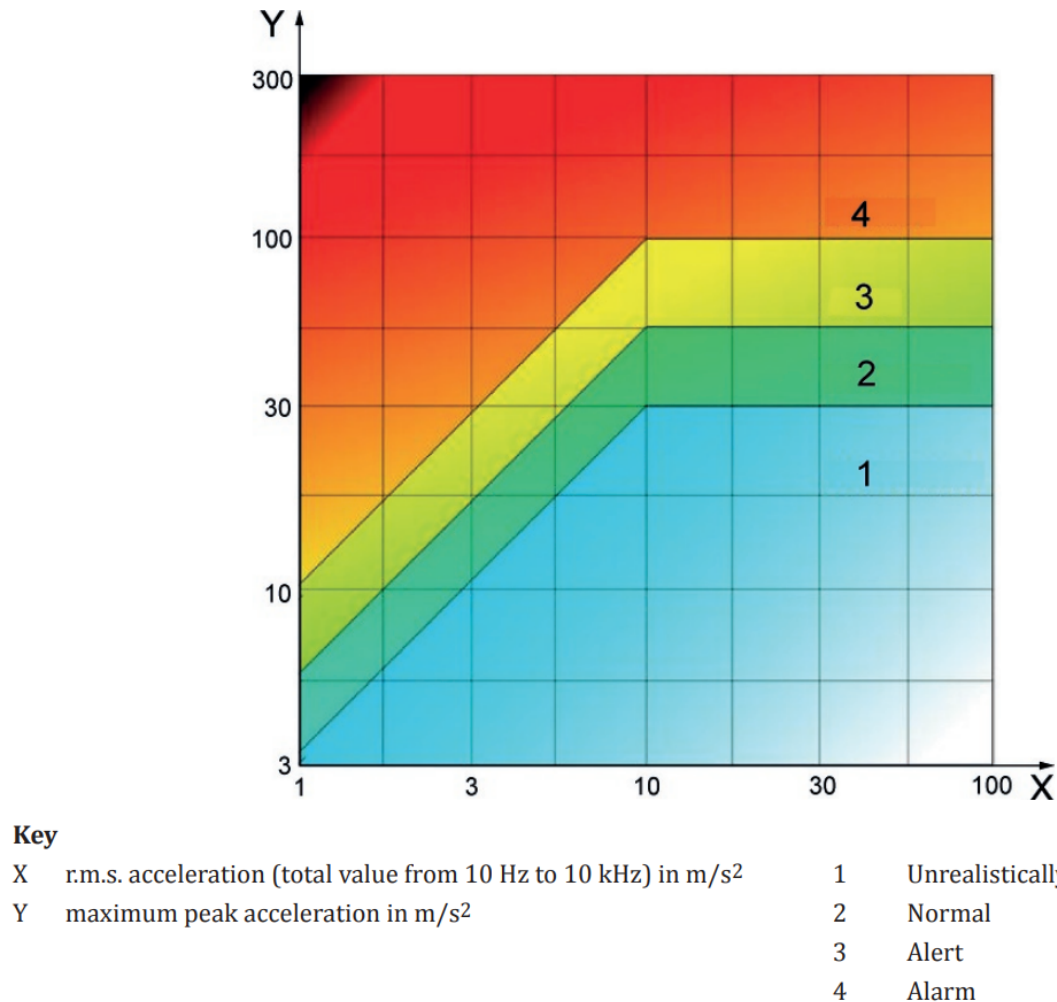


Figure 2.7: Bearing fault severity chart, reproduced from [25]

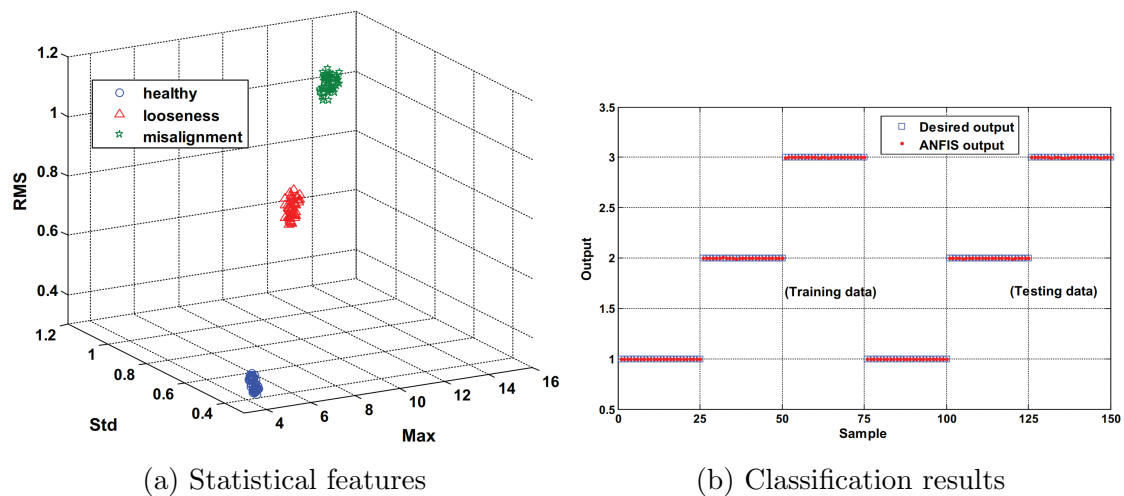


Figure 2.8: Implementation of ANNs with fuzzy logic for classification of water pump condition, reproduced from [39]

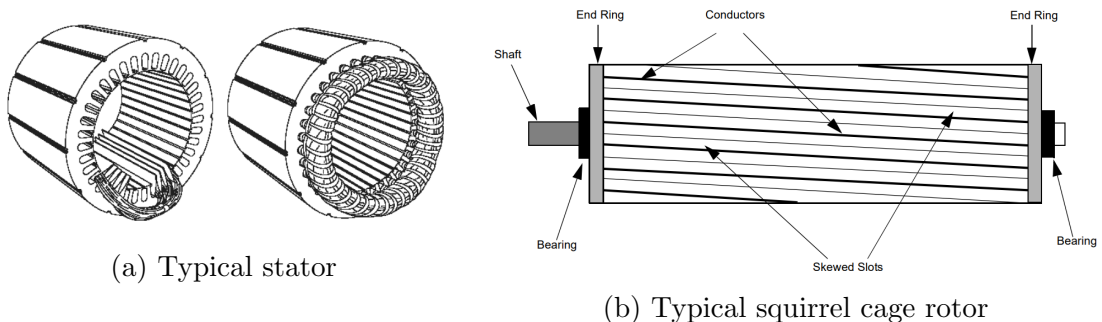


Figure 2.9: Typical elements of a squirrel cage induction motor, reproduced from [40]

Fault	Frequency	Notes/Causes
Shorted stator winding	$v.f_s \pm k.f_r$	Short circuit in stator windings
Broken rotor bar	$f_s \pm 2.k.s.f_s$	Motor can fail if numerous enough
Static rotor eccentricity	$v.f_s \pm k.RS.f_r$	Air gap eccentricity which can be very damaging to the motor
Dynamic rotor eccentricity	$v.f_s \pm (k.RS \pm n).f_r$	Air gap eccentricity
Mixed rotor eccentricity	$f_s \pm k.f_r$	Air gap eccentricity
BPFI	$f_s \pm k.f_r \frac{n}{2} (1 + \frac{d}{D} \cos\beta)$	Defect on inner race
BPFO	$f_s \pm k.f_r \frac{n}{2} (1 + \frac{d}{D} \cos\beta)$	Defect on outer race
BSF	$f_s \pm \frac{k.f_r.d}{2D} (1 - (\frac{d}{D} \cos\beta)^2)$	Defect on rolling element
FTF	$f_s \pm \frac{k.f_r}{2} (1 - \frac{d}{D} \cos\beta)$	Defect on cage

Table 2.3: Faults which can be detected with MCSA - mechanical rotor frequency f_r , supply frequency f_s , slip s , number of rotor slots RS, integers $k, n = 1, 2, 3\dots, v = 1, 3, 5\dots$, number of rolling bearings n , ball diameter d , pitch diameter D , bearing contact angle β , [32][41]

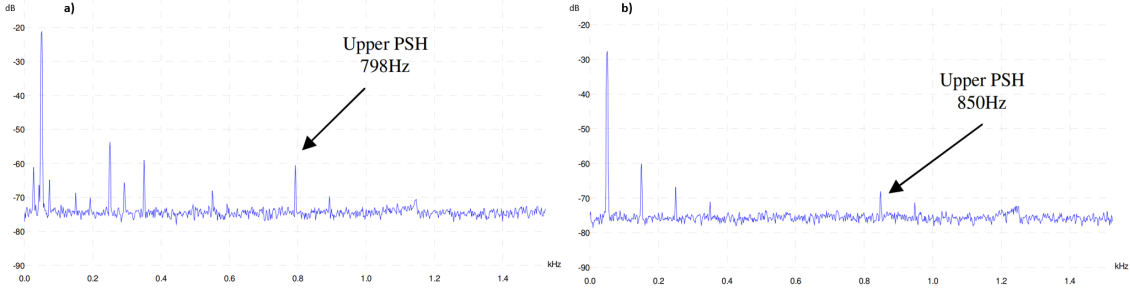


Figure 2.10: Healthy current signal for cage rotor induction motor with 36 slots, 32 bars and 2 pole pairs for a) loaded, slip = 6.4% b) unloaded, slip = 0, reproduced from [42]

common design being the three-phase rotor cage induction motor [40]. The two main components are the stator, which remains stationary, and rotor, which rotates (Fig 2.9). Around half the failures of induction motors are associated with faults on these two components, with another significant portion related to bearing failures [43].

The radial displacement induced by faults causes the air-gap between the rotor and the stator to vary, changing the reluctance and flux linkage. This can be detected through the stator current [32]. Electrical faults also have a direct impact on the stator current [44]. The stator current can be measured by placing a current sensor around the motor supply cable of a single phase [41]. The sensor does not have to be located close to the motor or power supply to measure accurately, providing an advantage over vibrational analysis [32].

The frequency spectrum is widely used to detect and diagnose faults in MCSA [44]. A peak at the supply frequency is expected and can be calculated by:

$$f_s = N_s \times \frac{120}{P} \quad (2.3)$$

where N_s is the synchronous speed of the motor in RPM and P is the number of poles on the stator [40]. This peak can be seen clearly at 50 Hz in the loaded and unloaded tests shown in Fig 2.10.

As seen from the list of fault frequencies in Table 2.3, many of the fault frequencies are similar to their vibrational counterparts but centred on the supply frequency [32].

A technique known as Park's Vector provides diagnosis through the time domain for three-phase motors [45]. The three-phase currents (i_A, i_B, i_C) are used to calculate the Park's Vector components:

$$i_D = (\sqrt{2}/\sqrt{3})i_A - (1/\sqrt{6})i_B - (1/\sqrt{6})i_C \quad (2.4)$$

$$i_Q = (1/\sqrt{2})i_B - (1/\sqrt{2})i_C \quad (2.5)$$

In ideal conditions, plotting the values of i_D and i_Q which correspond in time will give a circular locus centred at the origin. Faults such as shorted turns in the stator winding and broken rotor bars will distort the locus in its shape and thickness respectively (Fig 2.11) [45][46]. This method has been enhanced by work showing that the frequency spectrum of the Park's Vector modulus can be more effective for fault detection than simple FFT of the time signal [47]. The cost of this method is more sensors and computational effort to monitor three phases simultaneously.

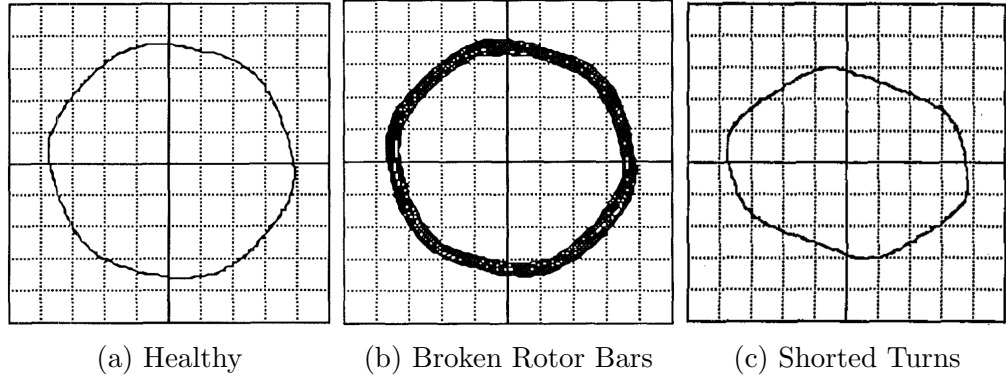


Figure 2.11: Park’s Vector for experimental current of three-phase, 4 pole, 50 Hz induction motor, reproduced from [45][46]

2.2.5 Prognostics

Prognostics is the final element in a complete CMS. It provides forecasts about the condition of machines into the future and therefore, crucially, the remaining useful life [3]. Having accurate forecasts increases the effectiveness of maintenance tasks and allow more efficient planning of resources [2]. Improvements in the accuracy of prognostic forecasts are a direct result of increased use of data-driven methods in other fields such as: Artificial Intelligence, Machine Learning (ML), Artificial Neural Networks (ANNs), fuzzy logic, unsupervised learning and Expert Systems [22]. Many of these techniques have been developed to find correlations in large amounts of data and are now being applied to CBM. A recurring challenge is properly defining system failure, which will vary significantly between applications [2][22].

The effective application of data-driven techniques is dependent on the quality of the data and it can be a challenge to obtain training data from commercial applications [2]. A recently developed machine learning application for denoising images without access to clean references could have an impact in noisy environments where it is hard to measure reference signals, and highlights the potential crossover in machine learning from other applications [48].

Physics-based models can provide information about how faults will presents themselves. Cracks and bearing spalling are faults which are hard to verify without causing damage to the machine but can be modelled precisely [22]. This approach is being investigated by as one of the projects supported by Lloyd’s Register.

Traditional methods such as fault tree analysis and Failure Modes and Effects Analysis (FMEA) have been combined with ANNs to build more accurate and useful CBM systems [5].

2.3 Condition Monitoring Systems

Implementing CBM requires having complete CMSs in place. A complete CMS contains sensors, processors, algorithms, communication channels and human readable outputs. It is important that such systems are accurate, reliable and work as part of the overall maintenance strategy [32]. Within the maritime industry, low cost and clear outputs will also be vital to uptake [13].

2.3.1 Existing Market Solutions

There are, of course, existing market solutions for CMS. One industry which has recently become focused on CBM is wind energy generation, due to the poor reliability of early wind turbines [8]. A compilation of commercially available CMSs for wind turbines highlights that modern systems are built in much the same way as those designed for relatively simple applications in manufacturing [29]. All of the systems surveyed were able to perform at least some level of diagnosis after a fault had occurred. However, large disparities were found between the capabilities of the systems.

An investigation by Lloyd's Register found that systems can be designed which fulfill the requirements for condition monitoring of marine pumps, but that the cost of such a system can be higher than the cost of the pump itself [10]. Single vendor solutions had upfront costs on the order of £10000, with additional costs through installation, licenses and software to follow. For large segments of the maritime industry, these costs are simply too high.

2.3.2 Embedded Systems

Embedded Systems describes a wide range of systems, generally comprised of microcontrollers with direct access to hardware. Within the IoT architecture, they are nodes which collect data using sensors, perform processing and transmit data to a central node [12]. This approach provides flexibility and speed during deployment at a relatively low cost [49].

There are several key factors which must be considered when designing an embedded CMS for industry:

- **Cost** - While the cost of individual node is low, effective condition monitoring implementations will require many nodes to be placed at different points of the machine or on different machines [12][28].
- **Processing power** - Powerful systems can use complex analytical tools to perform fault detection and diagnosis quickly, as well as providing more options for communication and user interaction [50].
- **Security** - There is a growing realisation that security of IoT devices must be enhanced to protect proprietary information and prevent deliberate misuse of devices for malevolent purposes [51].
- **Energy consumption** - Systems which only use small amounts of energy - on the order of 10 mW - can run independently with energy harvesting methods while sampling sensors in the kilohertz range [52].
- **Communication** - There is a wide variety of communication protocols available with different levels of complexity and resilience. Low-energy, wireless protocols such as Bluetooth and Zigbee offer flexibility but could be problematic to implement in noisy environments such as ships [53].

Fig 2.12 shows the software block diagram and built hardware of a wireless embedded system designed to detect faults on motor arrays [33]. This represents a typical wireless sensor approach, where data is collected and transmitted to a central

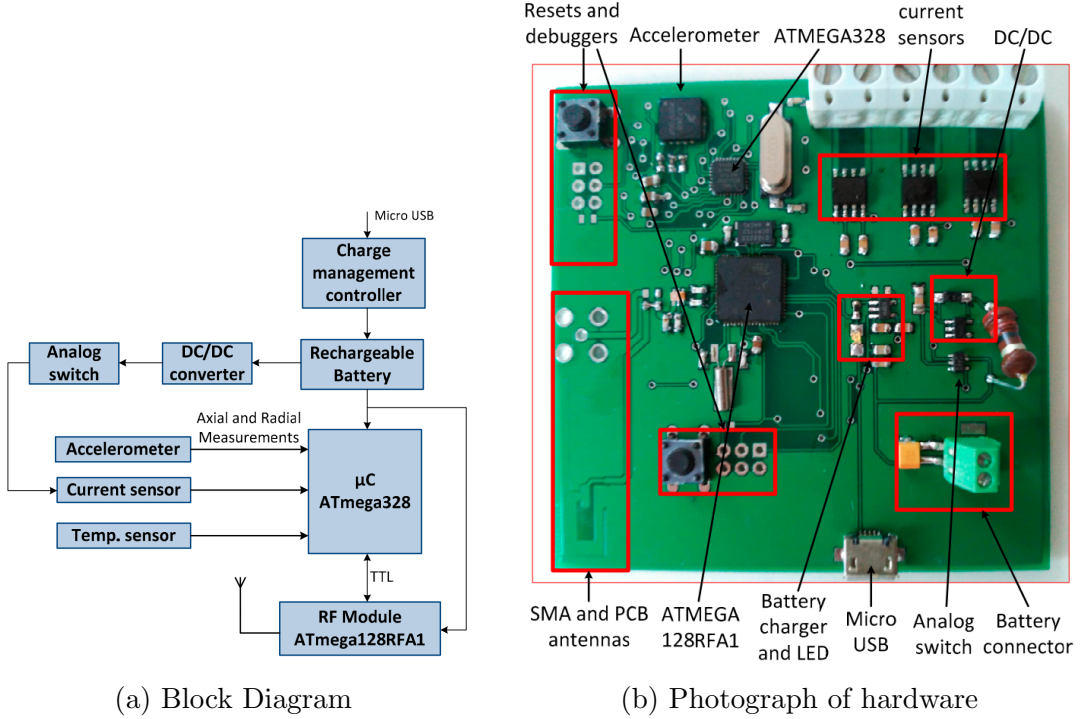


Figure 2.12: Wireless Sensor Node for monitoring and fault detection, reproduced from [33]

unit for further processing. No processing of the signals is actually performed on board.

The work presented in [12] and [49] demonstrates the potential of embedded systems to process information before transmission. Both systems are monitoring induction motors, but calculating different parameters. The system in [12] monitors all phases of a three phase motor, calculates the RMS current and voltage and transmits information about the power consumed to a central node. The central node collects data from several wireless sensors and compares it against user-specified limits to determine the condition of the machine. This work is poorly documented and it is not clear exactly how the embedded software is designed to work or how well the system has been validated.

The system in [49] is designed to calculate and transmit the torque, speed and efficiency of the motor. It shows good agreement between experimental tests and a reference model of the motor. The embedded software and system architecture is well laid out.

Sensors

The dramatic drop in the cost of sensors is an enabler for low cost embedded systems [9]. Microelectromechanical system (MEMS) accelerometers can cost as little as 10% the price of traditional piezoelectric counterparts, and have been shown to work well measuring amplitude and frequency of vibration [54]. They can also measure multiple axes in one device and perform signal conditioning [55]. A review of electric current sensors highlights increases in accuracy as new sensor types are developed [56]. Contactless current sensors and current clamps are widely used for MCSA as cables can remain intact [32].

Chapter 3

Fault Detection and Diagnosis with Offline Processing

This chapter tests methods for FDD, using offline processing from data collected on the Condition Monitoring Laboratory (CML) in the national Centre for Advanced Tribology at Southampton (nCATS). Using the CML provided two main advantages for the project:

- Test the ability of simple statistics to identify the condition of the machine with a sophisticated data collection system
- Compare the performance of the embedded system to sophisticated hardware and software

3.1 Condition Monitoring Laboratory

The CML was developed to demonstrate CM principles through vibration analysis and is the result of several individual projects, group projects and summer internships (Fig 3.1). The motor is a 3-phase squirrel cage induction motor with 4 poles, power consumption of 0.18 kW and runs at up to 1500 rpm [58]. Acceleration is measured on each bearing with Omega ACC786A accelerometers, which have a bandwidth of 14 kHz, sensitivity of 100 mV/g within a range of ± 80 g, resonant frequency at 30 kHz and is surrounded in an industrial casing [59]. The accelerometers are mounted with screw threads [57]. Data is collected at 5 kHz using National Instruments Data Acquisition Cards and sent to a PC for storage and processing. Motor speed is verified with a light-based tachometer.

Bearing 2 is mounted on a platform which can be pushed with a linear actuator to induce bending in the shaft. Some of the bending is absorbed by the coupling between the shaft and the motor which is flexible to allow quick assembly of the CML without the need for precise mountings. Exact calibration of the actuator is not possible due to the legacy control software.

3.2 Experimental Methodology

As the CML has been in use for several years, it is unlikely that it is in a completely healthy condition. To ensure a healthy condition for baseline measurements, new

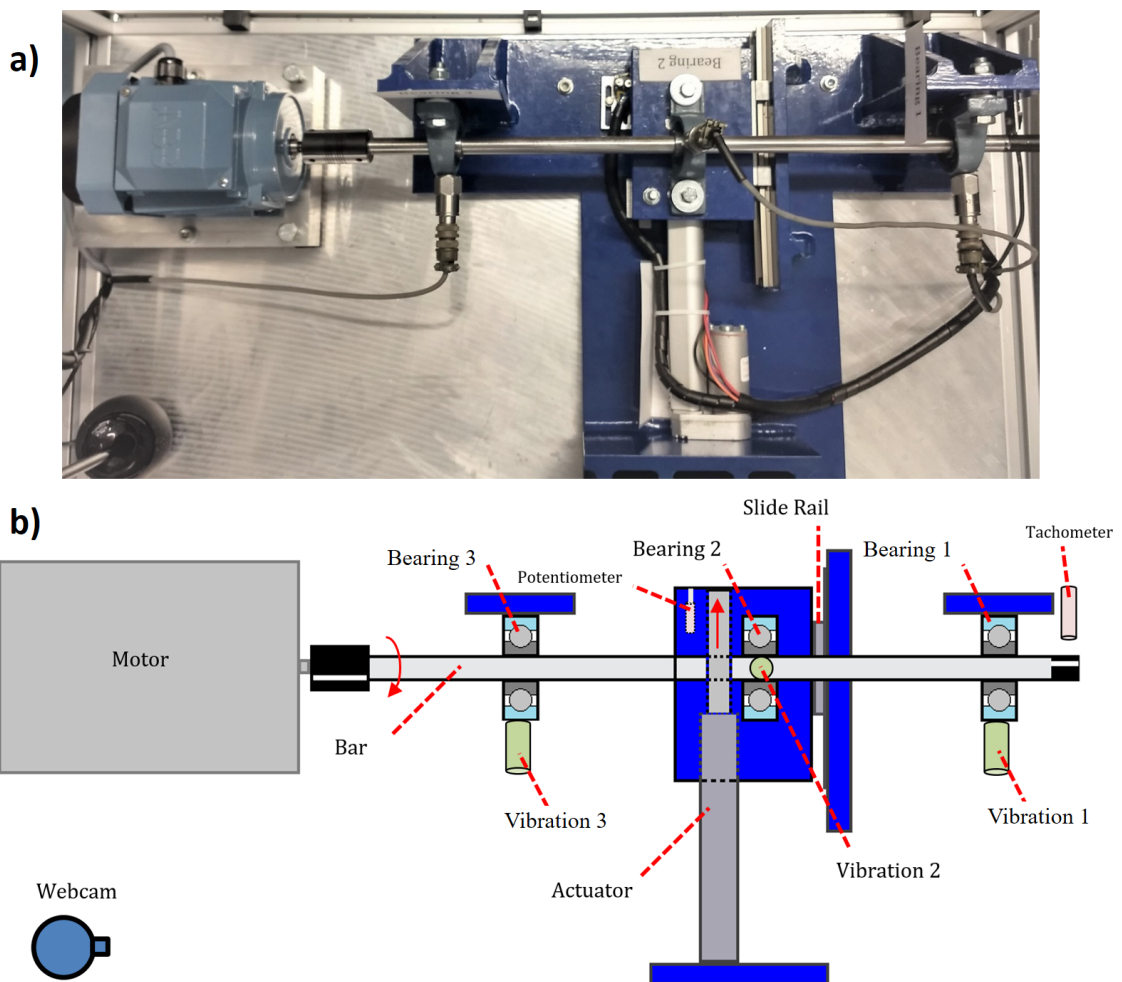


Figure 3.1: CML in nCATS Laboratory - a) Photo, b) Diagram, b) reproduced from [57])

bearings were fitted and the shaft was aligned carefully to reduce any bending. Data was collected from all three accelerometers for processing. Next, bending was induced in the shaft. Finally, the shaft was returned to the healthy condition, and bearing 3 was replaced with an older bearing which is thought to have damage. The bearing inspection process is destructive and was not possible within the timeline of this project.

By collecting information about the vibration at each bearing in three different conditions, processing of the data should reveal significant differences in statistics extracted from the frequency spectrum, as shown by Moosavian et al. [39]. Time domain statistics will also be compared to the ISO bearing fault chart [25]. The viability of the CML and individual accelerometer mounting points for further testing can then be assessed.

Acceleration data was sampled at 5 kHz for 5 seconds, and each condition was sampled 10 times. The sampling rate cannot be altered through the existing software. Each sample was transformed to the frequency domain before the maximum, RMS and STD of the frequency spectrum were extracted. The average values of these statistics were also calculated across the samples. The frequency spectrums were then averaged to remove transient signals.

The nCATS laboratory is busy and other experiments were taking place during testing. Therefore it is possible that some noise was introduced to the results from outside sources. However, given that the purpose of this project is to implement condition monitoring on a ship, an incredibly noisy environment, any techniques used should show resilience to noise [20].

3.3 Results

It is clear that the three conditions inspected have distinct vibrational signatures (Fig 3.2). These signatures also vary significantly on each of the different bearings. These results support the use of these statistical features for fault detection. Looking at only the values of maximum and STD, there is almost no overlap between the conditions, and simple inequalities are sufficient to classify them (Fig 3.3). The similarities to the results used for training of a neuro-fuzzy inference model suggest that the CML will be suitable for testing the embedded system and could provide a data set for ANNs or ML models in the future [39].

Closer inspection of the time data revealed that a significant DC component was affecting the results, particularly of Bearing 1 and Bearing 3. A DC component would result from gravity if not processed properly. It is possible that the software in the existing setup did not account for this component or that it resulted from imperfect fitting or calibration of the accelerometer. Fig 3.4 shows the results following extraction of this component by subtracting the mean value from each sample in the time domain. The maximum is affected as the largest component often was the DC component, which was not significantly affected by the changing condition. After removal, the maximum is closely related to the condition of the machine.

Bearing 2 provides the most clearly separated data. This was expected in the case of bending, as the bending force travels directly through the bearing, but it also detects the effect of bearing faults. As such, this bearing is most suitable for further investigation. The averaged frequency spectrum of Bearing 2 in the different conditions reveals significant differences (Fig 3.5). Although values were calculated

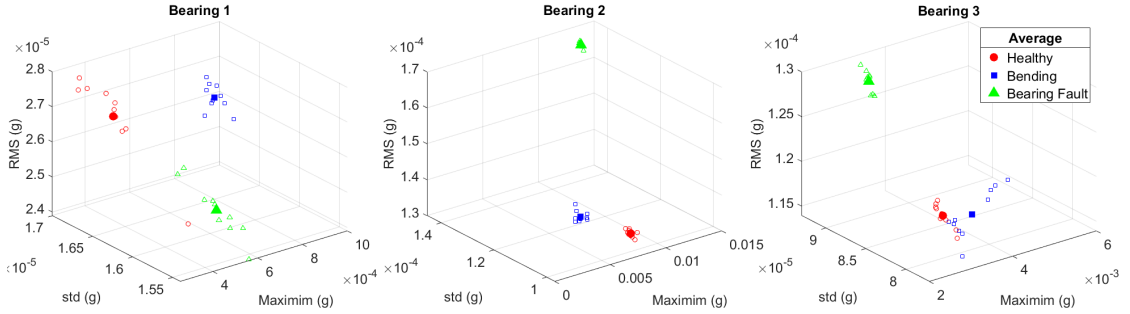


Figure 3.2: Results from investigation of existing condition monitoring setup

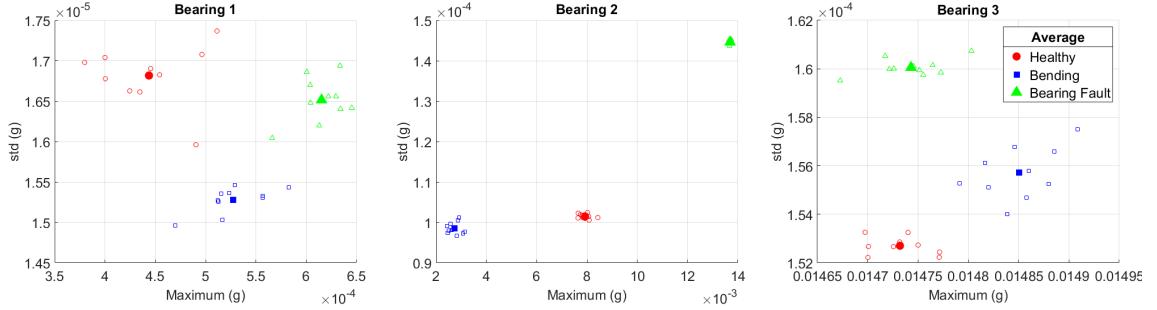


Figure 3.3: Results from investigation of existing condition monitoring setup with only maximum and standard deviation of the frequency spectrum shown

up to 2.5 kHz, there is nothing of interest beyond the range shown. The rotor frequency and its harmonics are visible for all conditions. With bending, the rotor frequency is diminished and its second and third harmonics are larger, as expected (Table 2.2). There is also more noise below 500 Hz. The faulty bearing signal is differentiated by a largely increased maximum at the rotor frequency. This could result from loose housing on the bearing. The rotor harmonics are also less distinct. All three conditions show a small peak at approximately 1160 Hz, which shifts to a slightly lower frequency under bending. The cause of this peak is not yet known, although it may be related to bearing pass frequencies.

Comparing the results to the chart of bearing fault severity provided by the ISO, the expected results are not seen (Fig 3.6). Firstly, the chart had to be extrapolated to lower values of acceleration to accommodate the measured values. Bearing 1 is still below these limits so is discounted. Bearing 2 and Bearing 3 both show separation in values between the conditions. However, the supposed bearing fault condition appears to be healthier than the healthy condition. With Bearing 2, the bent condition is on the border of the alarm values for a bearing fault. This suggests that there may be some issues using the time domain to diagnose faults.

This experiment validates the CML for testing of the embedded system. Bearing 2 has the most distinct vibration signatures so will be used for accelerometer mounting.

3.4 Evaluation

While the results from this experiment will be helpful to the development of the embedded system, there are some notes regarding the CML. It proved very difficult

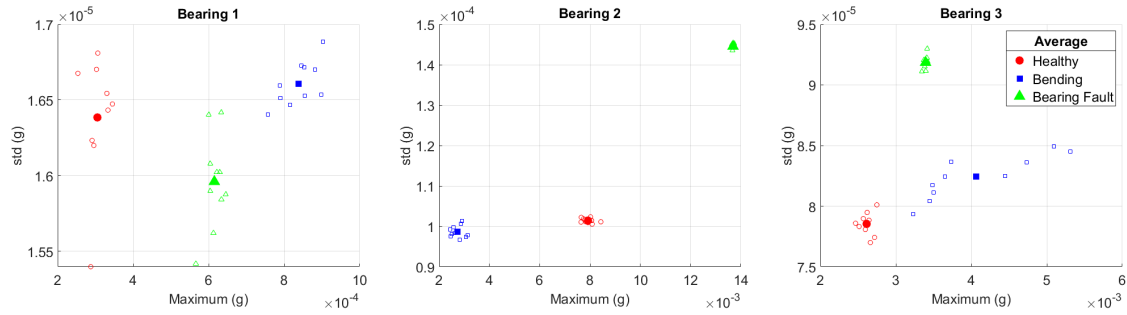


Figure 3.4: Results after removing DC frequency component

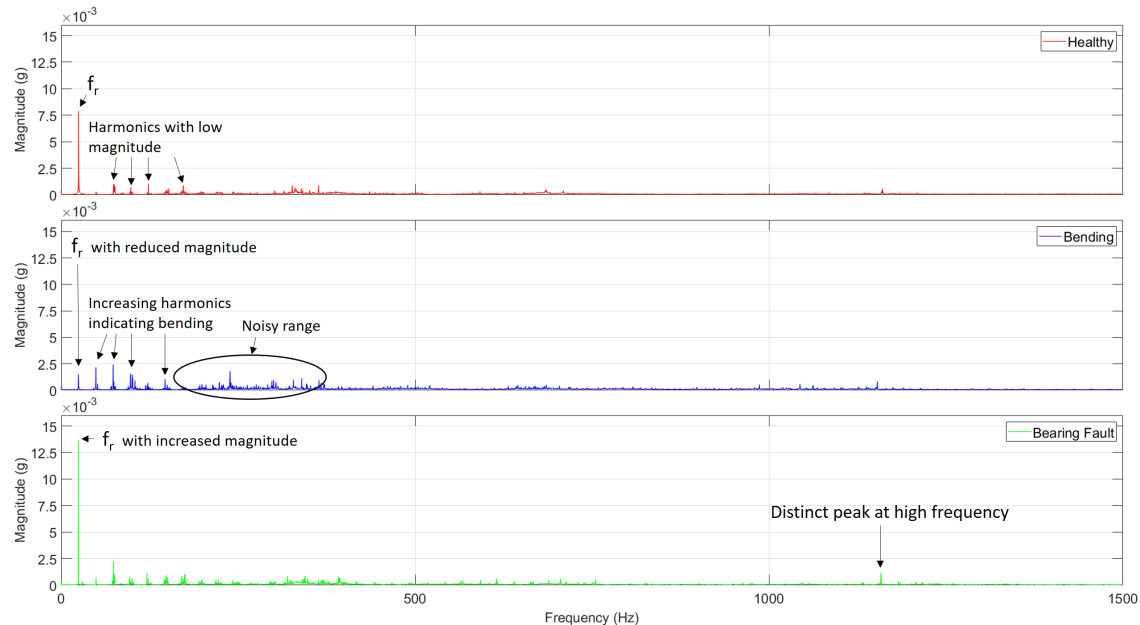


Figure 3.5: Averaged frequency spectrum for Bearing 2 of CML with annotations

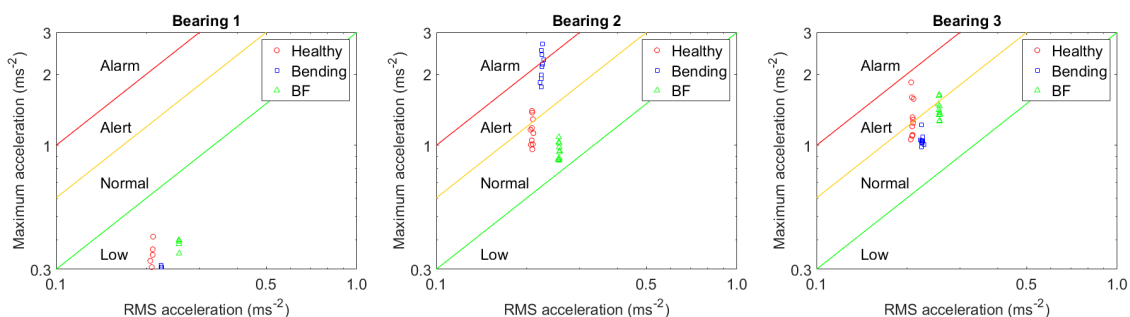


Figure 3.6: Comparison of results with ISO bearing fault chart

to replace the bearings due to the way the CML has been built. Small variations in the position of the bearings results in bending and it is difficult to exactly replicate healthy conditions. Linear actuator control needs to be improved in the future to allow for finer and more repeatable control. This follows suggestions that it be replaced by a stepper motor [57]. The entire CML is mounted loosely on a heavy metal top. It should be fixed in place to prevent movement of the bearing base or motor.

Chapter 4

Modular Development of Embedded System

Before an embedded CMS can be developed, it is necessary to test the individual elements in controlled conditions (Fig 4.1). This will lead to confidence in the implementation of more sophisticated techniques which are necessary for CM.

The processor used in this project is the MSP432P401R, mounted on a development board. It was chosen for its: ease of development; low cost; Precision ADC; hardware pin configurations; EnergyTrace technology [60].

4.1 Online Processing

Online processing of data is a key component of the embedded CMS. In addition to correctly transforming the signal from the time to frequency domain, statistics must be correctly extracted. As discussed previously, the parameters of maximum, RMS, and std have been chosen. To assess the implementation of the processing, data generated and processed in Matlab is sent to the board to compare the output of processing. It is expected that there will be some small differences in the results from the board and from Matlab. The computation in Matlab will use double-precision floating-point format, whereas, to conserve memory use, 16 bit integers are used on the microcontroller. The integers represent fixed point numbers and can suffer from both truncation and overflow errors [61]. Fixed-point FFT has been studied and shown to have good accuracy, with mitigation strategies available to improve the signal-to-noise ration if necessary [62][63]. To allow direct comparisons of processing, the time domain input will be stored in integer values for both the board and Matlab.

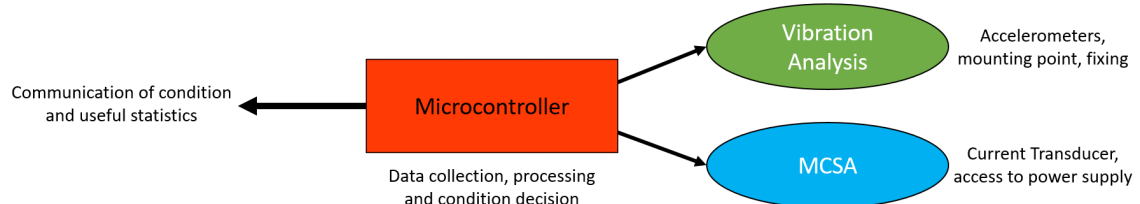


Figure 4.1: Modular elements of embedded system for condition monitoring

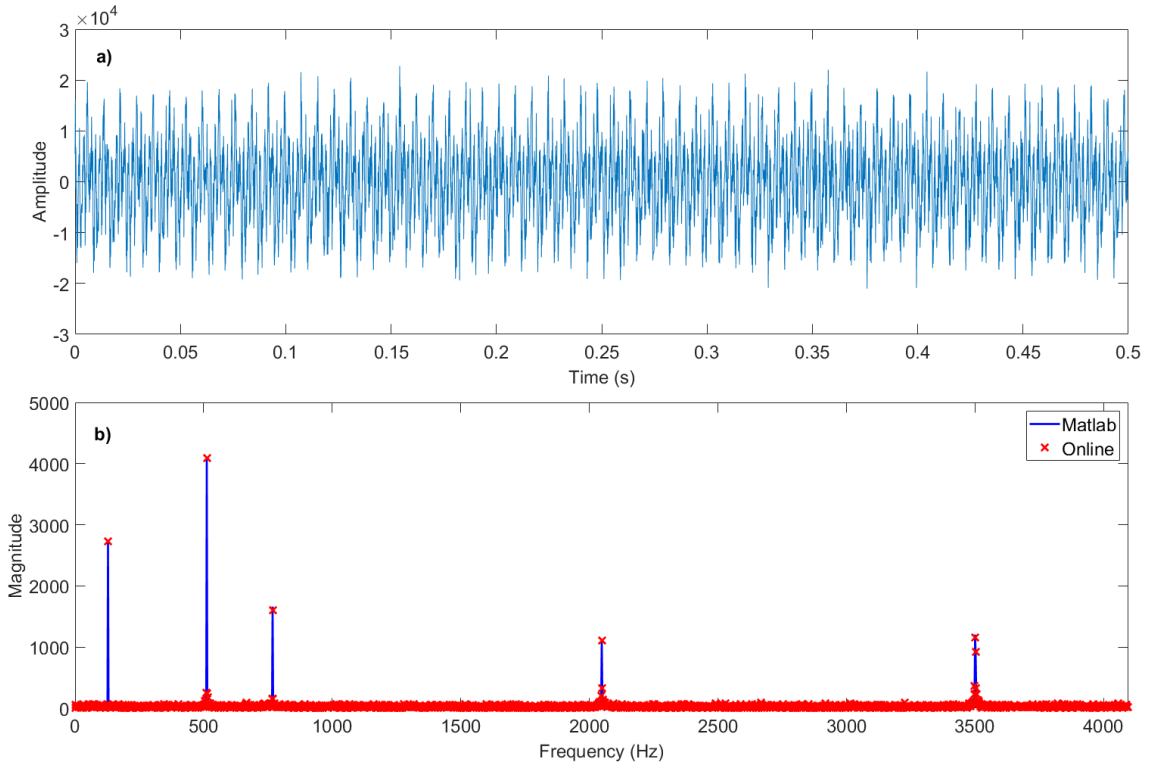


Figure 4.2: Processing of frequency spectrum online and in Matlab - a) Time signal, b) Frequency spectrum

The online implementation uses the KissFFT library which is publicly available under a BSD license [64]. KissFFT uses an out-of-place, time decimation, mixed-radix FFT and provides optimisation for even length real signals. It also provides improved capability over freeware provided by the CMSIS-DSP library which limited the length of the time signal to 1024 [65]. There is no such limit with KissFFT which allows full use of available memory. The MSP432 has 64 KB of SRAM [60], so the theoretical limit for the sample size is $(64000/3/2) = 10667$ - 1 array of real numbers as input, 1 array of real numbers and imaginary numbers each as output, and 2 bytes each for 16 bit integers. However, the practical limit was found to be closer to 6000, due to how SRAM data and memory is allocated on the MSP432. A sample size of 4096 is used as it provides an exact fraction of the available sampling rates and therefore a sensible resolution in the frequency domain.

Results

The results of processing a noisy time signal with multiple components provide evidence that online processing is accurate (Fig 4.2, Table 4.1). Limitations of this test are that the time signal is relatively simple, with five frequency components and noise. At low levels of magnitude, online processing does not agree exactly with the Matlab output, however this does not interfere significantly with statistic extraction.

Statistic	Matlab	Online
Maximum	4078.20	4126
RMS	127.27	128
Standard Deviation	122.05	123

Table 4.1: Statistics of frequency spectrum calculated online and in Matlab

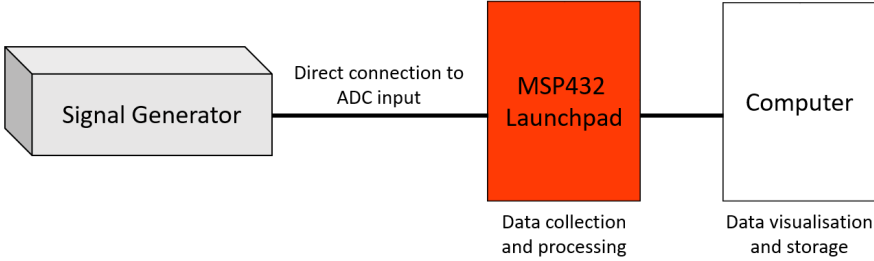


Figure 4.3: Test setup for ADC measurements

4.2 ADC

Having demonstrated the accuracy of online processing, the next step is to combine it with analog inputs at specific sampling frequencies. Many accelerometers and current sensors provide analog outputs only so verifying the accuracy of this module is key to obtaining reliable data from more complex measurements with peripherals.

MSP432 has an Analogue-to-Digital Converter (ADC) which measures with 14 bits (0 - 16833) and can be triggered from a number of internal clocks [66]. While the advertised maximum sampling rate is 1 Million Samples Per Second (MSPS) it was found through experimentation that the most accurate timing source is the internal low-frequency oscillator in its 32.768 kHz mode. Due to the way the timing trigger works for the ADC, the maximum sampling frequency with this oscillator is 16384 Hz, giving a Nyquist frequency of 8192 Hz. While this is less than the 10 kHz range recommended for full condition monitoring, it will still be effective for diagnosing a wide range of faults and performing other condition monitoring services [28][20]. The ADC measures from 0 V to V_{cc} , which is 3.3 V for the MSP432 [66].

To test the ADC, a Rigol DG1062Z signal generator provided sinusoid signals directly to the analog input pins of the MSP432 (Fig 4.3). Frequencies were chosen to be offset by 53 Hz to avoid harmonics of the supply frequency [54]. The amplitude of the signal is 1 V peak-to-peak and offset by 1.5 V to prevent breaching the limits of the ADC. The DC component produced by the offset was removed during pre-processing of the time signal online - subtracting the mean of the time signal from each value. Model sinusoids were generated in Matlab for comparison, with the same sampling frequency and scaling the amplitude by $(V_{pp}/V_{cc}) * bits_{adc}$.

Results

The results of the frequencies tested are shown overlaid on a single graph, against the peak value calculated by the model (Fig 4.4). There is good agreement with the model signals. In particular, the frequency is identified well and the amplitude is

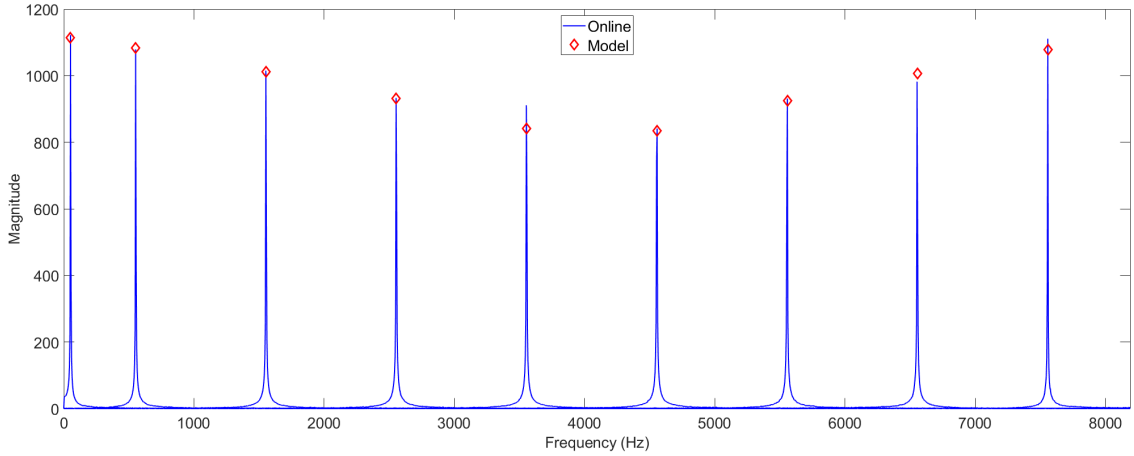


Figure 4.4: Frequency spectrum of signals measured with ADC and processed online compared to model

	A	B	C
Sensitivity (mV/g)	800	400	40
Frequency Range (kHz)	0.400	1.500	11
Amplitude Limit (g)	± 1.5	± 2	± 50
Resonant Frequency (kHz)	6.0	2.4	21
Shock Limit (g)	5000	5000	10000
Unit Price (£)¹	N/A ²	38.15	73.76

Table 4.2: Properties of MEMS accelerometers [67][68][69]

similar for most values. It can be seen that there are no peaks between the measured frequencies, indicating that both the measurement and FFT functions are working as expected. It was found that at frequencies above 6 kHz, the amplitude of the signal measured was not constant with time. This suggests small inaccuracies with the ADC at higher frequencies. Overall, this experiment demonstrates functionality of the embedded system for measuring and evaluating signals across a range of frequencies relevant to condition monitoring.

4.3 Accelerometers

Three accelerometers suitable accelerometers were identified (Table 4.2). They were chosen to have significantly different bandwidths, the frequency at which response is -3 dB from the true value. They also have a range of sensitivities. All three provide analogue output and operate at 3.3 V.

To test the devices, the accelerometers were vibrated at a known frequency and

¹Unit price for single evaluation board at large UK electrical retailer

²No longer on sale

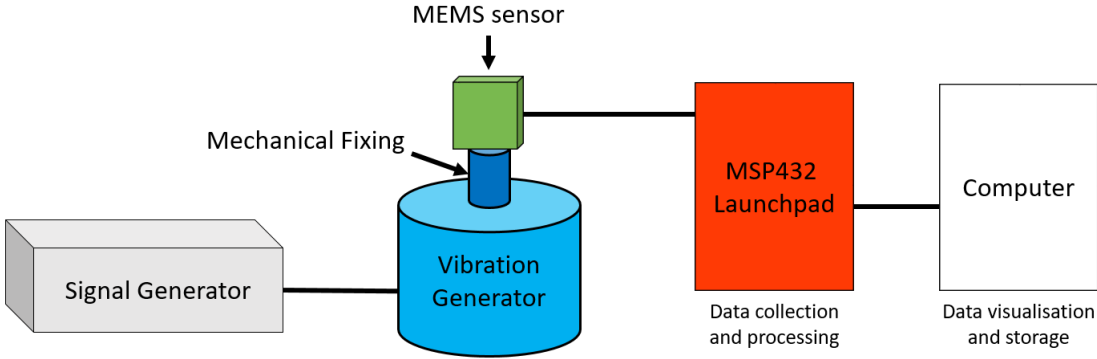


Figure 4.5: Test setup for MEMS accelerometers



Figure 4.6: Banana plug mechanical fixing for MEMS sensors on vibration generator

power and their responses compared, similar to methods described in [54][55]. The setup is shown in Fig 4.5. A Rigol DG1062Z signal generator is connected to a Frederiksen 2185.00 Vibration Generator. The vibration generator can vibrate at signals from 0.1 Hz to 5 kHz with amplitude of 7 mm at low frequencies and decreasing with frequency [70]. Sinusoidal signals were generated to provide a clear signal. A specially manufactured banana plug (Fig 4.6) provided a strong mechanical fixing for the accelerometers to ensure accurate readings [36]. As the accelerometers were mounted on evaluation boards, screw holes closest to the sensors were used to mitigate the effects of resonance of the boards themselves, although this effect could not be completely removed. The sensor output was connected to the MSP432 analog input, which collects data and performs data processing on the signal. The time data and frequency signal were then sent to a computer for data visualisation, storage and further processing.

The main subject of interest is how the accelerometers respond at different frequencies. To avoid interference from the mains frequency, the frequencies chosen were offsets of 53 Hz [54]. A low frequency within the frequency range of all the accelerometers was tested, followed by multiples of 500 Hz. The signal generator was set to a peak-to-peak voltage of 5 V which was found to produce vibrations of approximately $\pm 1g$ RMS. Beyond 2553 Hz, the acceleration increased significantly

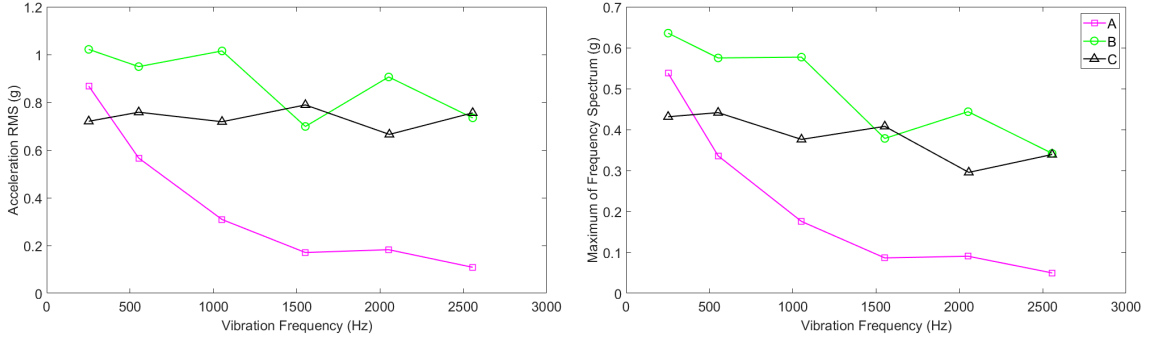


Figure 4.7: Comparison of RMS of acceleration and maximum of frequency spectrum for MEMS sensors across frequencies

beyond the range of two sensors, so testing was limited to these frequencies.

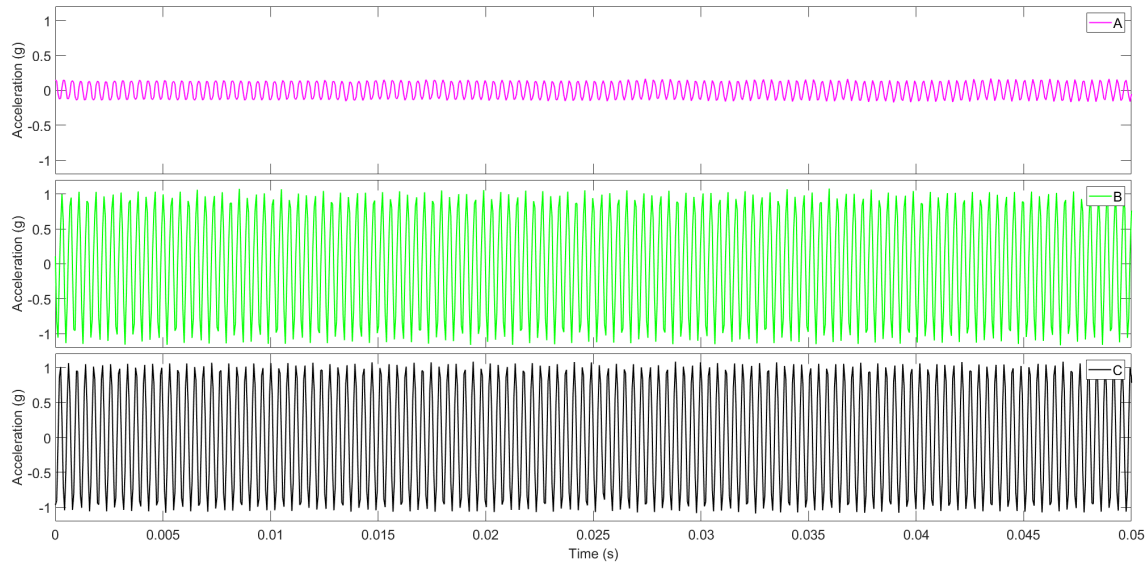
Accelerometer output was sampled at 16384 Hz, significantly higher than the highest frequency to be tested. Each sample collected 4096 measurements, giving a frequency resolution of 4 Hz. Three samples were collected from each accelerometer at each frequency, and the RMS acceleration and maximum of the frequency spectrum was averaged across the samples. Using RMS and averaging the frequency spectrum are both methods which will reduce the effect of noise in the measurements and allow the true performance of the sensors to be assessed [3]. ADC values were converted to standard units using the theoretical sensitivities listed in the datasheets of the accelerometers [67][68][69]. It is expected that MEMS A will show attenuated response at high frequencies compared to MEMS B and C due to its lower frequency range. Effects due to resonance may also be visible in the higher frequency tests of MEMS B [68]. Inaccuracies are expected for C as the acceleration is small compared to the range of the sensor and resolution will therefore be lower than A and B.

The experiment was performed in the Hardware Lab in Zepler Building at University of Southampton. Other experiments were being performed at the same time which could contribute noise to the results. The temperature inside the lab is maintained at a constant temperature of 22°C, but variations in temperature could also add inaccuracy to the measurements.

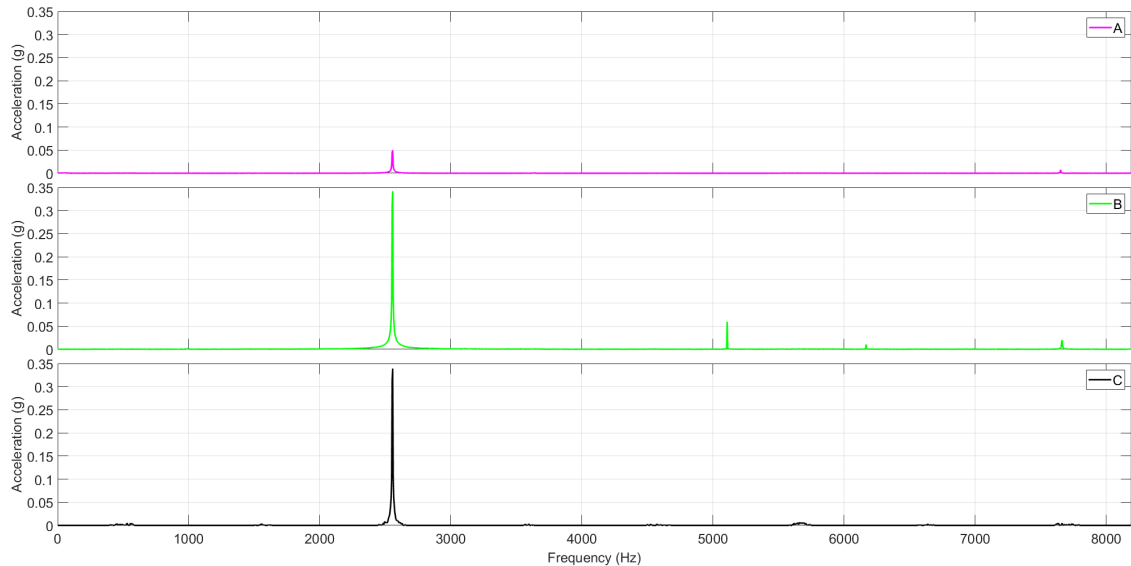
Results

The accuracy of the sensors cannot be directly derived from this test, as the exact acceleration produced by the vibration generator is not known. However, MEMS C provided the most constant values for acceleration RMS and frequency spectrum maximum, followed by B (Fig 4.7). As expected, A performed similarly to the other sensors at the low frequency within its range but then quickly gave attenuated responses. MEMS B and C had extremely similar responses at 2553 Hz, beyond the listed frequency range of B. While it is promising that the calculated values were so close, the fact that this value beyond the frequency range of B suggests that it may not be entirely accurate.

Close inspection of the test at 2553 Hz (Fig 4.8) highlight properties of the accelerometers which were also visible at other frequencies. The time data for B and C is very similar and clean, and the attenuation for A is significant. All sensors correctly identified the frequency with a sharp peak, and also showed some noise around 7.6 kHz, suggesting there may be harmonics produced by the vibration



(a) Sample of time signal



(b) Averaged frequency spectrum

Figure 4.8: Results of accelerometer tests at 2553 Hz

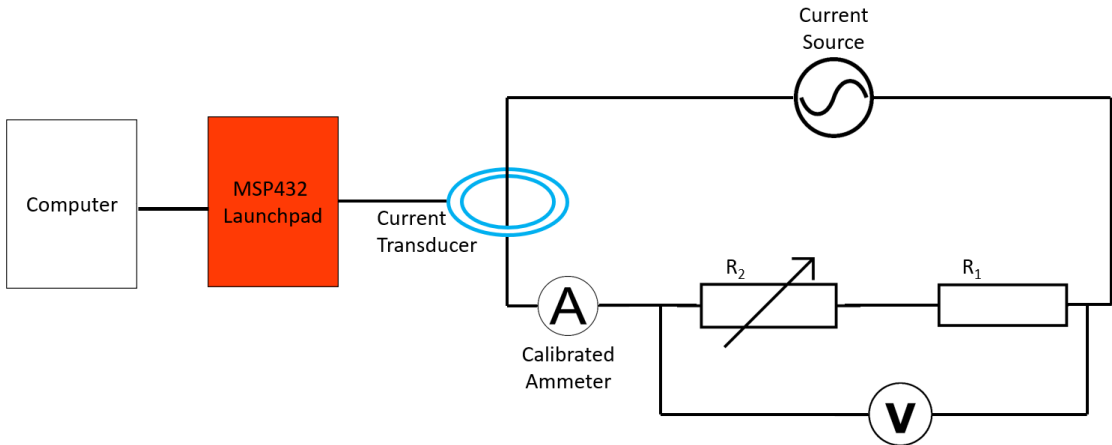


Figure 4.9: Test setup for validation of current transducers

	CT1	CT2
Sensitivity (mV/A)	76.67	13.333
Frequency Range (kHz)	250	100
Current Range (A)	± 20	± 150
Supply voltage (V)	3.3	5
Unit Price (£)³	6.82	10.52

Table 4.3: Properties of Current Transducers [71][72]

generator. B shows small peaks at several harmonics, possibly a result of the sensor harmonics or the board. C shows harmonics and sub-harmonics, likely a result of noise given their small amplitude.

This experiment should be repeated on a calibrated vibration generator where the acceleration is known.

These results suggest that MEMS C will be the most accurate and effective sensor for the embedded system.

4.4 Current Sensors

Two Current Transducers (CTs) were selected as candidates for the embedded system (Table 4.3). A wider range of available sensors were found to be available than for accelerometers. The sensitivity of the sensors varies largely, allowing for the embedded system to monitor the current of differently sized motors on board ships. Both CTs selected are open loop, hall-effect probes which can be easily applied to a variety of motors, needing only to isolate a single phase. The frequency range of both CTs is above what is required for condition monitoring, providing the capability in hardware for future advancements of the system focusing on higher frequencies. Notable differences between the CTs is the current range and supply voltage. Having a large current range allows for application to a wider range of

³Unit price at large UK electrical retailer

machinery, including larger pumps found on board ships, at the possible cost of decreased accuracy for lower power machines. A supply voltage of 5 V, required by CT2, can be accommodated by the embedded system, but to allow full use of the current range circuit protections and scaling of the signal would be required - the embedded system will use 3.3 V analogue reference voltage and signals beyond that range could cause damage.

The sensors were tested by generating an AC current and passing it through resistors to generate a known current level (Fig 4.9). Step down transformers were used to provide large currents at mains frequency (50 Hz in UK) and around 30 V peak. Large ceramic resistors with sizeable heat sinks were connected in series with a variable resistor and an ammeter to adjust the current to the required values. A moving iron AC ammeter certified to half a percent provided confidence in the current value [73]. The CT was then placed around the wire connecting the ammeter to the current source. A voltmeter was connected across the load for safety and to note any anomalies.

The current was set to 1 A, 2 A and 3 A and three samples were taken for both sensors of 4096 measurements at 4096 Hz. A lower sampling rate was chosen than for the accelerometers to provide increased resolution around the supply frequency. The data was transformed to the frequency domain online. Time and frequency data was transferred to a computer for further processing and storage. The average RMS of time signal was calculated across the three samples and converted to SI units using the theoretical sensitivity of the sensors. The measured sensitivity was then calculated using the known current values for comparison. The frequency spectrums were also averaged to remove impulses and other local effects.

A large peak is expected at 50 Hz with some small peaks at harmonics. Other experiments were taking place in the High Voltage Zepler Laboratory so could provide a source of noise in the data. There could be some variation in results due to changes in temperature.

Results

The CTs performed very differently. CT1 provided very clean results (Fig 4.10) with little visible in the time or frequency domain. CT2 showed noisy and diminished signals in both the time and frequency domain. The frequency spectrum shown for both CTs has been abbreviated to the area of interest, no useful signals were seen above 200 Hz. Both sensors clearly highlight the expected peak at 50 Hz with no sign of significant harmonics.

The calculated and measured sensitivities of the sensors are listed in Table 4.4. CT1 performed very closely to its theoretical sensitivity, whereas CT2 had a much lower measured sensitivity than its theoretical value. This could be due to the relatively low current compared to the range of CT2, or could be a result of sensor inaccuracy.

This experiment should be repeated at higher currents and with varying supply frequency to evaluate how the CTs perform across a wider range of frequencies.

These results suggest that CT1 is the more appropriate CT for the embedded system, assuming that the current requirements are within its range. Beyond that current range, CT2 can still be expected to accurately describe the shape of the frequency spectrum, although its scale may not be relied on as heavily.

Current (A)	CT1		CT2	
	RMS (A)	Sensitivity (mV/A)	RMS (A)	Sensitivity (mV/A)
1.0	1.001	77.3	0.665	8.9
2.0	2.014	77.2	1.273	8.5
3.0	3.024	77.3	1.820	8.1

Table 4.4: Results of Current Transducer testing

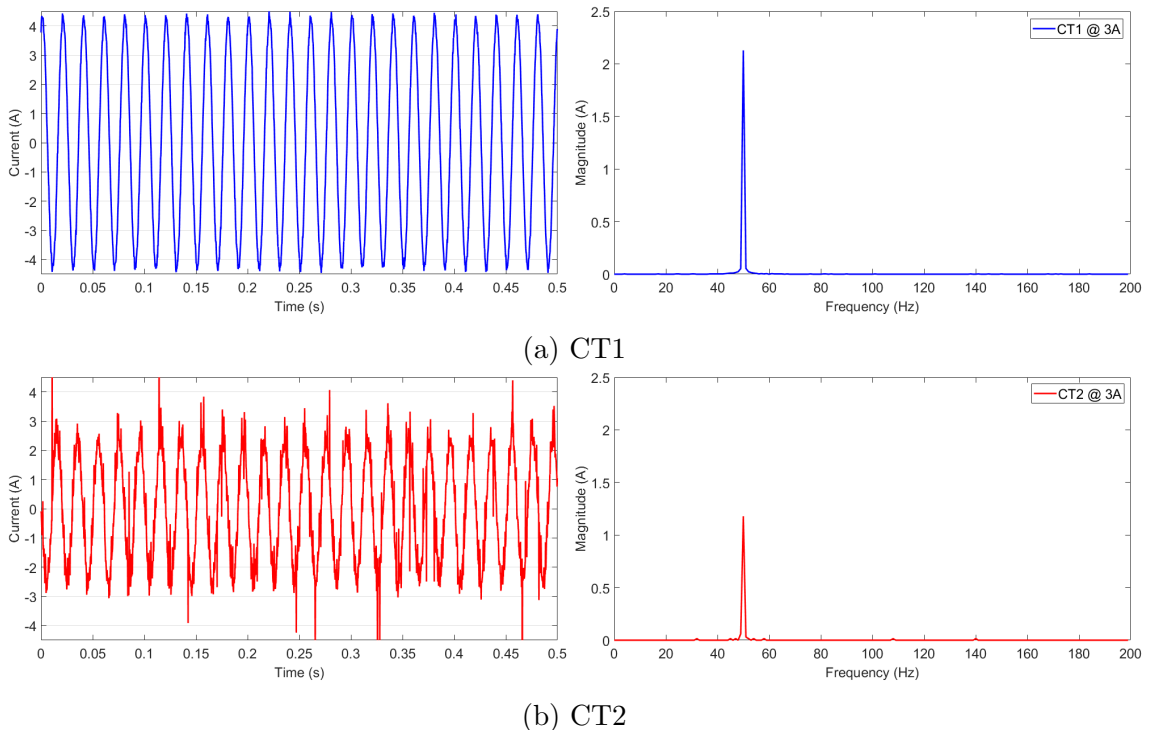


Figure 4.10: Current test at 3A

Chapter 5

Validation of Embedded Systems Approach

Before designing the embedded CMS, the sensors and processing implementation were tested on the CML for comparison to each other and, where possible, to a reference sensor on the existing system. In addition to gaining more information about the sensors, these tests will also allow an evaluation of the relative merits of MCSA and vibration analysis for condition monitoring of the CML. These tests also provided an environment to improve the design of embedded CMS hardware and software.

5.1 Vibration Analysis

5.1.1 Sensor Comparison

Following the work in Chapter 3, vibration analysis is a promising candidate for condition monitoring of the CML. It is also clear that there are significant differences in how the available MEMS sensors perform, particularly at frequencies in the kHz range. Testing on the CML allows for an informed decision about which sensor to use in the final design.

The CML was placed into a healthy condition. As noted, the exact condition of the CML is hard to control, so to provide a baseline for comparison of the sensors, measurements were also taken from the existing accelerometer, referred to as *ref*. Bearing 2 was chosen due to its ability to give clear information about machine condition. Five samples were taken with each sensor. For the MEMS sensors, the frequency spectrum was calculated online and transferred to a computer. The *ref* sensor values were stored on the CML computer and processed offline. Average frequency spectrums across the samples were calculated. The *ref* sensor was sampled at 5 kHz. To ensure that all frequency components measured by the *ref* sensor were included, the MEMS sensors were sampled at 8192 Hz.

A mechanical screw fixing was used, which allowed the evaluation boards to be attached in a similar manner to the banana plug used previously (Fig 5.1). Two washers were used to prevent the end of the bolt from pressing on the bearing casing and influencing the vibrations. The MEMS and *ref* sensors were all mounted using the same hole, diminishing the effect of mounting on the vibration signal.

The averaged frequency spectrums show good agreement with *ref* for MEMS

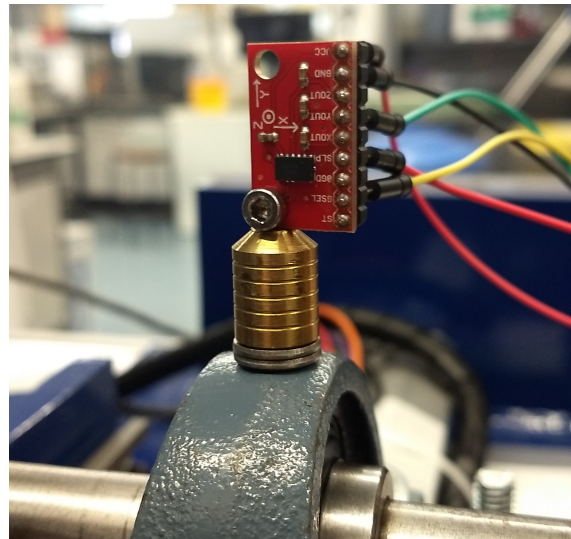


Figure 5.1: Mechanical fixing for MEMS sensors on bearing

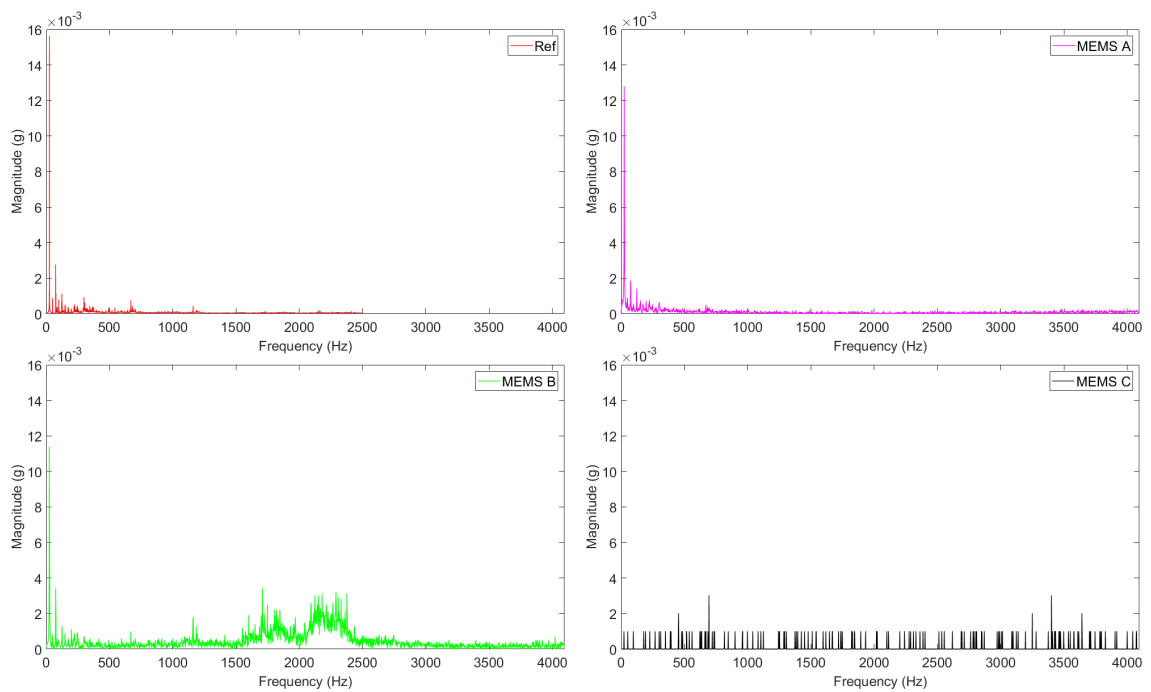


Figure 5.2: Comparison of *ref* and MEMS sensors

A and B at the lower frequencies, while MEMS C clearly struggles to detect the vibration signals (Fig 5.2). This is simply a result of the vibration level being too low for the sensor to discern signals from the motor from background noise. While MEMS C had been found to be a good candidate, the sensitivity is too low for the signals on the CML. This provides a clear reminder of the importance of adapting CMSs to the specific implementation. Further, there is a large amount of noise in the spectrum of MEMS B from 1500 to 2500 Hz. The frequency response curve for this sensor shows a rise in magnitudes for frequencies in this range before a steep decline [68]. However, this level of noise was not observed during initial sensor testing. Offline processing of the data found that some of this noise could be removed with a low pass filter at around 1 kHz, however this would remove the possibility of identifying frequency components at higher frequencies. MEMS A better characterises the frequency spectrum of the bearing, with a magnitude closer to *ref* at the rotor frequency and a less noisy signal overall.

Therefore, MEMS A is selected as the accelerometer for the embedded CMS and will undergo further testing.

5.1.2 Condition Monitoring

To inform the final system, the MEMS A and *ref* sensors were tested on the CML in different conditions. Again, healthy, bent and faulty bearings are the conditions. This would help identify differences in the signals and the ability of MEMS A to differentiate between the conditions.

Five samples were taken in each condition, with the sensors being tested one after the other without interfering with the CML to prevent small differences in condition. Time data was also plotted against the ISO bearing fault severity chart [25]. The remaining parameters are the same as the previous test.

It is expected that there will be some small differences between sensors. The *ref* sensor collects more samples and therefore has a higher resolution, as well as a higher frequency range. This should lead to a more accurate frequency spectrum. However, it was found that the statistics of the spectrum lead to clearly identifiable groups when plotted; this is expected also in the data from MEMS A.

Samples of the time data collected are shown in Fig 5.3. There is good agreement between the sensors in terms of magnitude and overall signal shape. The bent condition is clearly identifiable by a large amount of noise. Signal magnitude increases significantly for the *ref* sensor but not for MEMS A. Differences between the healthy and faulty bearing state are much harder to identify in the time domain.

The frequency domain provides further evidence that MEMS A performs similarly to the *ref* sensor (Fig 5.4). The spectrum for all three conditions is very similar between the sensors. Interestingly, MEMS A also performs well above its frequency range of 400 Hz, which was not seen in modular testing. This is indicated by noticeable peaks in the bent condition spectrum above 400 Hz, although there is a loss of accuracy compared to *ref*. The bent spectrum also shows noise at around 2 kHz for *ref* and 2.6 kHz for MEMS A. While this is well above the frequency range of MEMS A, the sampling rate is much higher. It is possible that the peak seen for *ref* is a result of aliasing and should actually be located closer to 2.6 kHz. However, this cannot be validated without further testing of *ref*, which is not the focus of this project. The similarity of the results suggests that MEMS A will be effective for

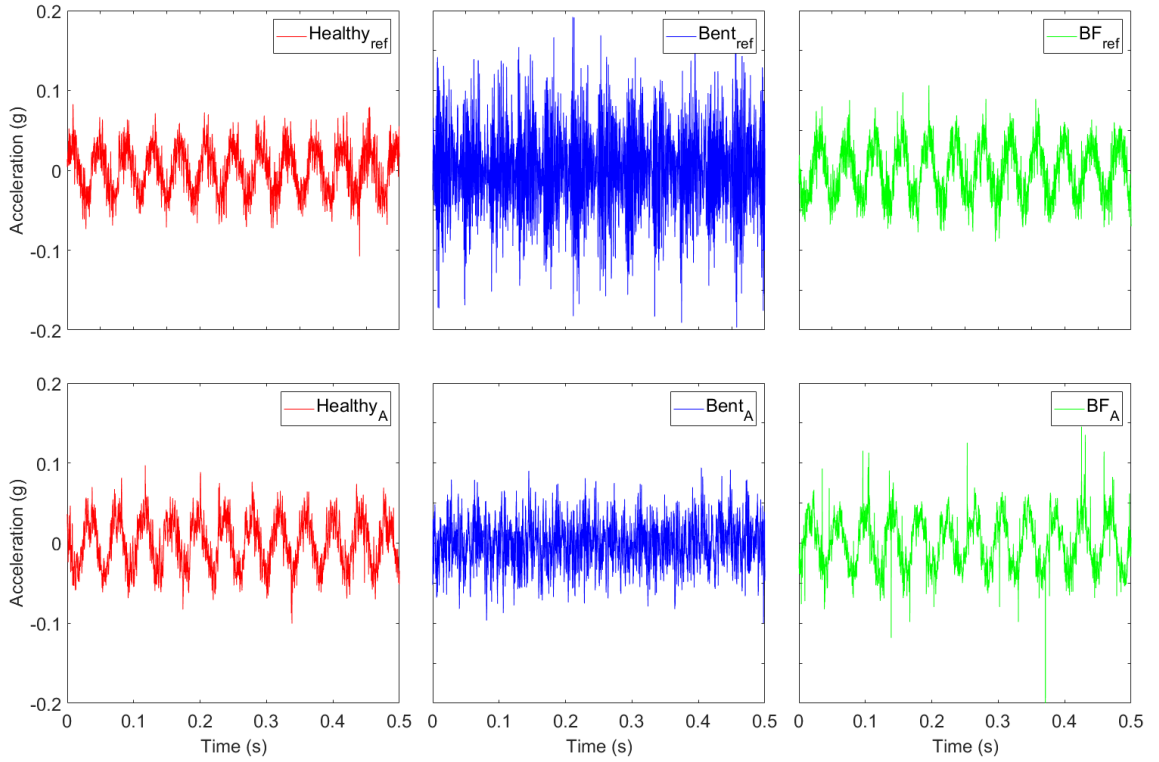


Figure 5.3: Time domain measured by *ref* and MEMS A sensor for different conditions

classifying the condition of the CML.

Extracting statistics from the frequency spectrum shows that the bent condition is easily identifiable for both sensors (Fig 5.5). As seen in the initial tests of the CML, the maximum value drops significantly. The healthy and bearing fault tests are much closer, although the individual readings remain tightly grouped, particularly for MEMS A. The sensors occupy a similar area of the state space, while not completely overlapping, and correspond well with each other. One peculiarity is that the bearing fault shows a lower maximum value than the healthy condition for *ref* and a higher value for MEMS A. Importantly, however, there is a clear difference between the three conditions tested.

Finally, statistics from the time domain are plotted on the ISO bearing fault severity chart (Fig 5.6). There are clear differences between the performance of the sensors, with MEMS A providing more accurate diagnosis. The *ref* values suggest that all three conditions fall within the ‘Normal’ boundaries. MEMS A shows the healthy and bent conditions very close together, in the ‘Normal’ range, while the bearing fault data falls into the ‘Alert’ range. It can be seen that the RMS values for all three conditions are similar, but the maximum value is much higher for the bearing fault condition. This is a result of impulses caused by the bearing fault. Therefore, the bearing fault severity chart provides a good method for the embedded CMS to distinguish the bearing fault condition, and MEMS A provides accurate information and diagnosis.

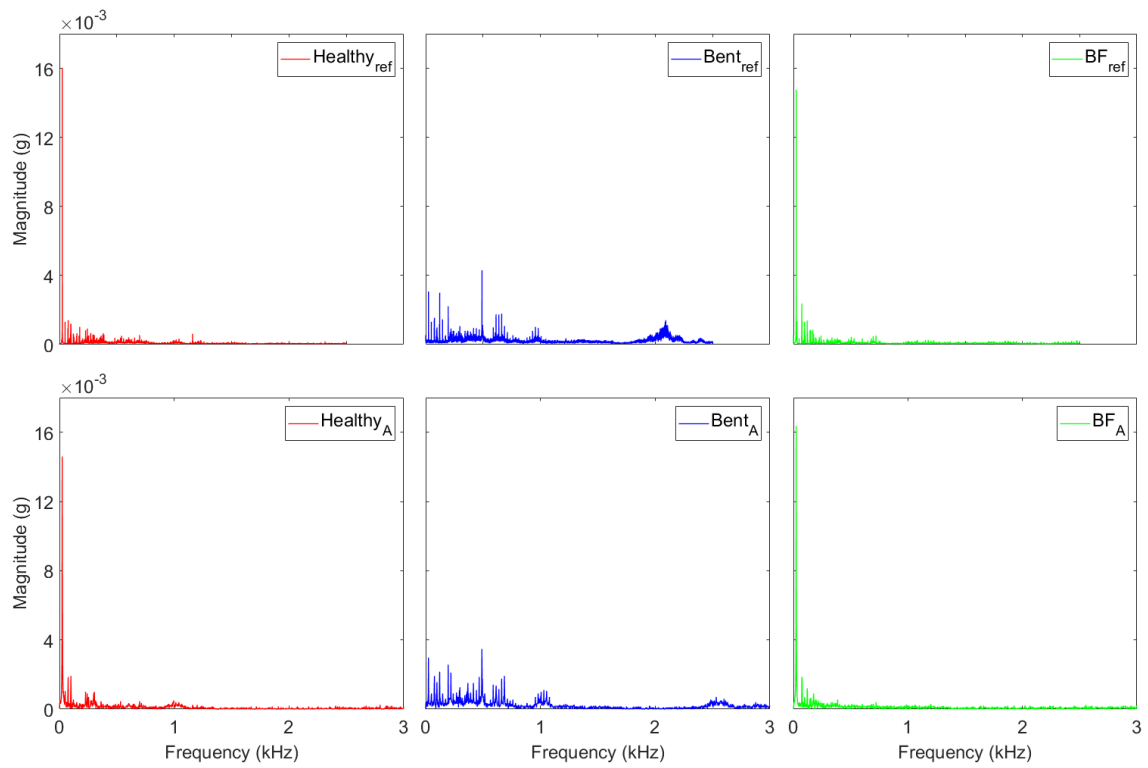


Figure 5.4: Frequency domain measured by *ref* and MEMS A sensor for different conditions

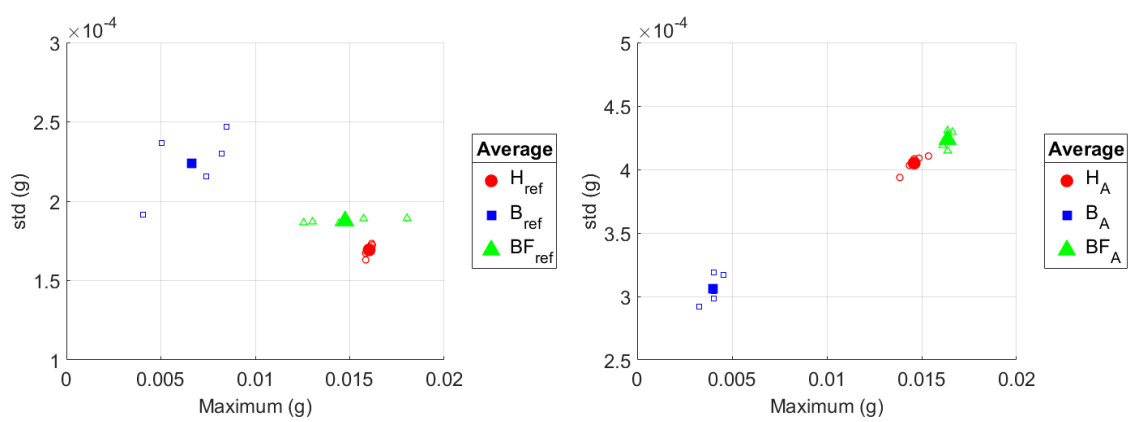


Figure 5.5: Comparison of statistics from *ref* and MEMS A sensors

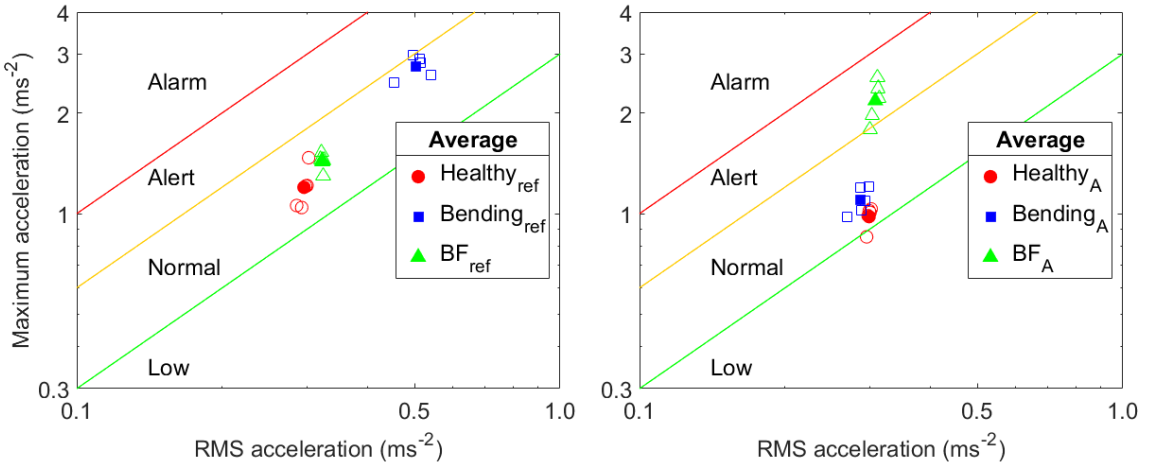


Figure 5.6: Comparison of statistics from *ref* and MEMS A sensors against ISO bearing fault chart

5.2 MCSA

As MCSA is not implemented on the CML, it is not possible to directly compare the results of any of the following MCSA tests to a data which is known to be accurate. Testing was conducted with this in mind and an effort to define what the limits of MCSA are for the CML and the embedded CMS.

5.2.1 Phases

Firstly, it was prudent to verify that all three phases powering the motor were working similarly. This should be the case in a healthy motor, but deviations could be caused by faults in either the motor or power supply [44]. Both CTs measured the motor in a healthy condition five times on each phase. The average RMS value in the time domain of the five samples was calculated. The theoretical sensitivity was used to convert the sensor output to SI units. The measured sensitivity calculated previously could not be guaranteed to hold in the new conditions of the nCATS laboratory and being close to a power supply with a large heat sink. A sampling frequency of 4096 Hz was used as the supply frequency of the phases was expected to be around 50 Hz.

The results, shown in Table 5.1, indicate that there is not a significant difference in current consumption across the phases. As before, CT2 shows lower current values than CT1. The range of current values is very small compared to the range of CT2, so the effective resolution of the sensor is diminished. All of the values are well within the current limit of 0.70 A specified in the motor datasheet [58]. Future tests and condition monitoring implementations can use any of the phases for MCSA on the CML.

5.2.2 Condition Monitoring

Next, the CTs were evaluated for their ability to discern between different conditions of the motor. MCSA can be a powerful technique for diagnosing issues with electrical components [44]. However, it should also provide information about the mechanical

Sensor	RMS Current (A)		
	Phase 1	Phase 2	Phase 3
CT1	0.297	0.296	0.293
CT2	0.248	0.252	0.263

Table 5.1: RMS current of motor phases during healthy operation

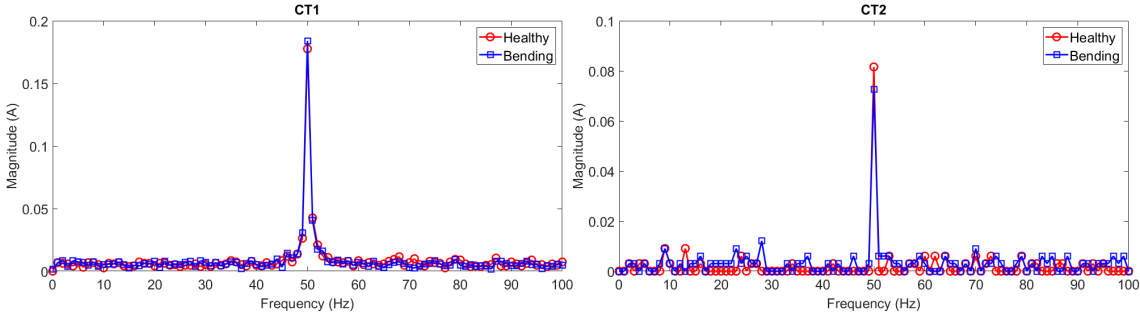


Figure 5.7: Frequency spectrum of CTs in different conditions

faults which can be easily tested on the CML.

The CML was tested in the healthy and bent conditions. The frequency spectrum, calculated online, was taken for five samples in each condition. Averaging of the frequency spectrum from the samples was performed offline to remove noise and allow for a clear distinction between the conditions. If the bending condition can be detected, it may appear as a heightened value at the supply frequency as a result of the motor load increasing from increased resistance acting on the bent shaft. Sampling frequency of 4096 Hz was used.

Both CTs showed very similar frequency spectrums for the healthy and bending condition (Fig 5.7). Due to its increased sensitivity, CT1 is able to more accurately define the spectrum, reinforcing the similarity between conditions. Frequencies above 100 Hz are not shown as there were no discernible peaks found in the test data. The peak of the spectrum has a diminished value in CT2 compared to CT1. This is due to the increased effect of noise for the sensor with a lower sensitivity.

Given the result of this test and the difficulty in changing bearings on the CML, it was decided not to perform a test for detection of bearing faults using MCSA. Therefore, MCSA will not be included as a direct input for condition monitoring in the final system design. In the future, MCSA should be investigated further on the CML for its ability to detect electrical faults. In the meantime, it can still be used to provide useful information.

5.2.3 Speeds

As condition monitoring on ships is currently very poor, even simple information can be of use [20]. This can be as simple as runtime of the motor, which Lloyd's Register understand is not recorded in many instances. Fortunately, MCSA is well prepared to monitor running time and speed of the motor, as the motor can only run with a large amount of current which will be detected. With no significant peaks in the frequency spectrum other than supply frequency, MCSA can reliably detect

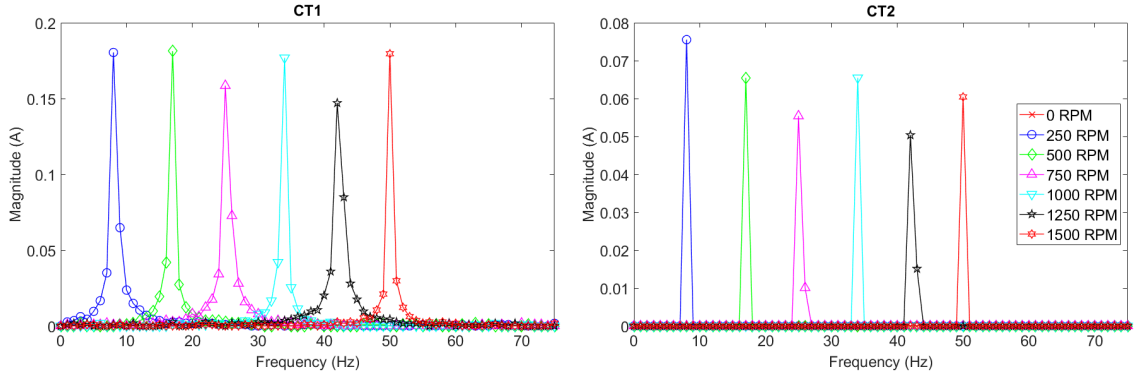


Figure 5.8: Frequency spectrum of stator current measured by current transducers at various motor speeds (legend shared)

running speed. This cannot be relied upon as readily with vibration analysis, as there are other significant peaks and the rotor frequency cannot be guaranteed to be the largest, making detection of rotor speed more difficult.

To test the CTs for this purpose, three samples were taken at each speed available on the CML - multiples of 250 RPM from 0 to 1500 RPM. The frequency spectrum, calculated online, was recorded and averaged across the samples. Sampling frequency of 4096 Hz was used.

Both CTs showed the ability to reliably detect discern the peak and therefore, the running speed of the motor (Fig 5.8). Note that although it is included in the results graph, the frequency spectrum of the 0 RPM test is not significant, suggesting that there is not a lot of noise in the stator current of the CML. The frequency range shown is limited as there is no significant information in the higher frequencies.

The sampling frequency and sample size limit resolution to 1 Hz, or 60 RPM. This is reasonable for the CML as it has been designed to only operate at multiples of 250 RPM. A higher sampling frequency would allow detection of faults, which may be relevant in the future. However, the requirements of the embedded CMS are dependent on the system being monitored and it may be necessary to increase the resolution if more precise rotor speed information is needed. With current hardware, the sampling frequency would have to be lowered.

5.3 Evaluation

As was found previously, vibration analysis offers good diagnosis capabilities for the CML. Unexpectedly, MEMS A sensor showed the best correlation with the *ref* sensor, of the available MEMS sensors. It also showed a superior ability over *ref* to diagnose bearing faults. Statistics from the frequency domain provide good diagnosis for the bent condition. The bearing fault severity chart provides a clearer diagnosis of bearing faults. Both the time domain and frequency domain should be analysed in the embedded CMS. MEMS A will be used and can be expected to provide accurate information.

While it is clear that MCSA offers limited information about the condition of the CML, it will provide value to the embedded system. By using stator current to monitor motor speed, runtime can be measured, providing useful information to users. Moreover, vibration analysis can then be selectively performed when the

motor speed is known to be at the same speed as during testing. This will help to prevent misdiagnosis due to varying motor speed. CT1 showed clearer signals and has a higher effective resolution for this CML due to its smaller current range. CT1 will be used in the embedded CMS.

Chapter 6

Embedded System for Online Fault Detection and Diagnosis

Having evaluated the CML at nCATS, and the ability of low cost sensors and hardware to classify conditions, an embedded CMS is presented. The design is discussed, including the philosophy behind the software design. A long term test is performed, attempting to simulate more realistic conditions. The energy use of the final system is measured and inspected.

6.1 System Design

6.1.1 Hardware

The embedded CMS includes elements of MCSA and vibration analysis (Fig 6.1, 6.2). Therefore, it uses CTs and MEMS sensors. For the purposes of this project, one sensor of each is used, although more could be added in the future for a more complex machine or more complex analysis. Additionally, to emulate an industrial system and increase the safety of the system, the CT has been soldered to long wires and the connections insulated with heat shrink (Fig 6.3). This allows the CT to sit inside the motor control box, which is connected to high power lines. The CT wires travel safely from the box to the MSP432 which sits inside the CML casing. In a working environment, such as on board a ship, there are strict electrical standards which wiring must adhere to [74]. To prevent noise from interfering with signals, shielded and twisted core cables should be used. Communication and power is provided by a USB cable which extends into the casing. This means that the system can be fully operated remotely. The safety of testing is improved and requirements of the system more realistic.

6.1.2 Software

The software for the system follows the flow chart laid out in Fig 6.4. Interrupts are used to trigger readings and capture ADC data. Reading triggers are:

- **Real-Time Clock** - Triggers a reading once every minute
- **Serial Interface** - Triggers a reading upon reception of certain messages

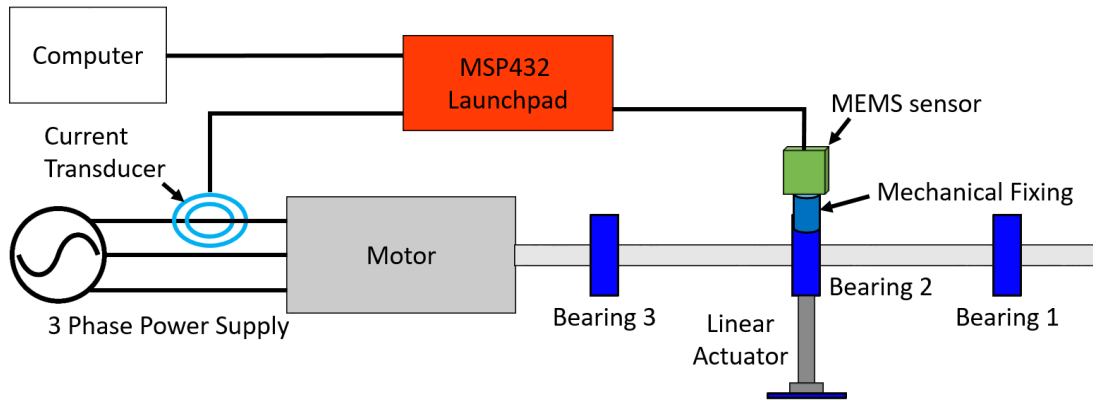


Figure 6.1: Diagram of embedded CMS setup for test on CML at nCATS

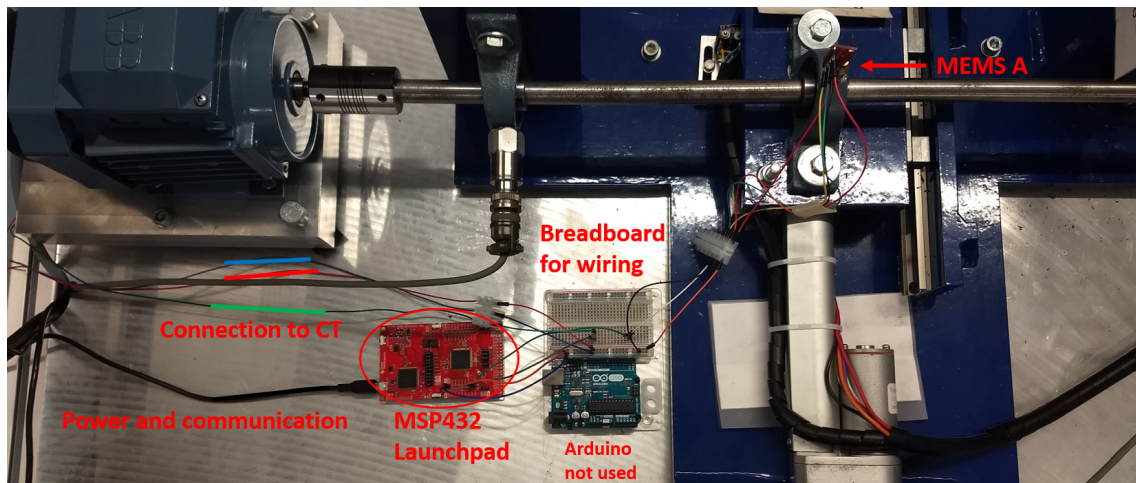
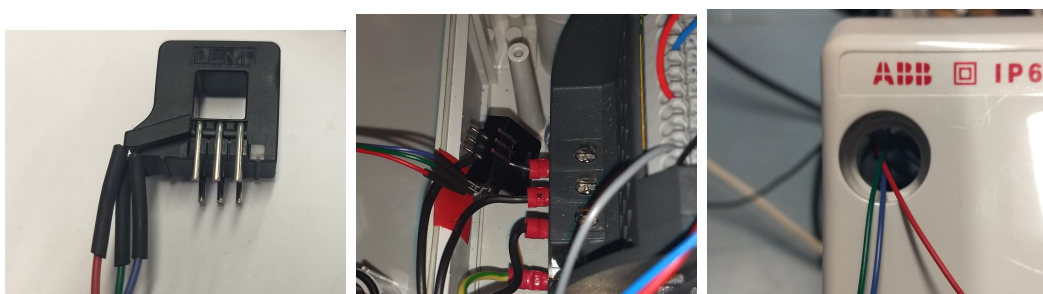


Figure 6.2: Photo of test setup on the CML at nCATS



(a) Heat shrink on CT con- (b) CT mounted inside mo- (c) Wires connected safely
nections tor control box to CT

Figure 6.3: CT setup for testing of embedded CMS

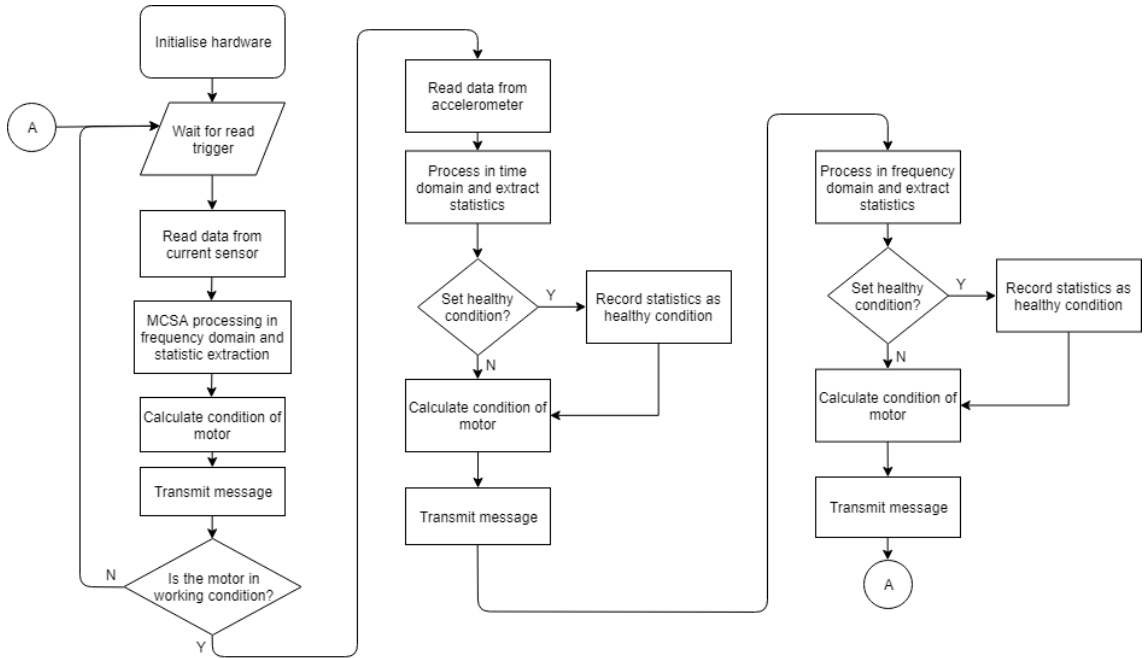


Figure 6.4: Software flow chart for embedded CMS

- **Push Button** - Useful for sanity checks

Once a new reading is triggered, the current sensor is sampled first at 4096 Hz. If the motor is found to be running at full speed then vibration readings are also triggered. A message containing MC SA information is transmitted.

If vibration readings are triggered, the accelerometer is read at 8192 Hz. Both the time domain and frequency domain are inspected and condition decisions are made. If an instruction to set a new healthy state has been detected, this information is recorded. Messages with vibration analysis information are transmitted.

While the transmitted information could be processed by a central node to provide diagnosis, all processing and decisions are performed online.

6.1.3 Condition Decisions

The main output of interest from the embedded CMS is condition. The algorithm for this classification is basic but based on the information generated by the tests on the CML.

The CT is used to identify the motor speed. The maximum of the frequency spectrum is identified. If it is found to be below approximately 0.04 A, the motor is identified as being stopped, as the main component is far below the magnitude expected from a running motor. If the maximum is above this level, the maximum frequency is used to identify the state of the motor. Between 48 and 52 Hz, the motor is identified as running, giving some allowance for error in measurements or calculation. Below that, a loading state is identified. During loading, it is expected that the motor is either starting up or stopping. Above 52 Hz is unexpected behaviour and the motor is identified as unhealthy.

Vibration analysis is used in both the time and frequency domain. Classifications are made with respect to ‘Healthy’ values which are set during operation. ‘Healthy’ values create a baseline against which changes can be measured. Limits are made

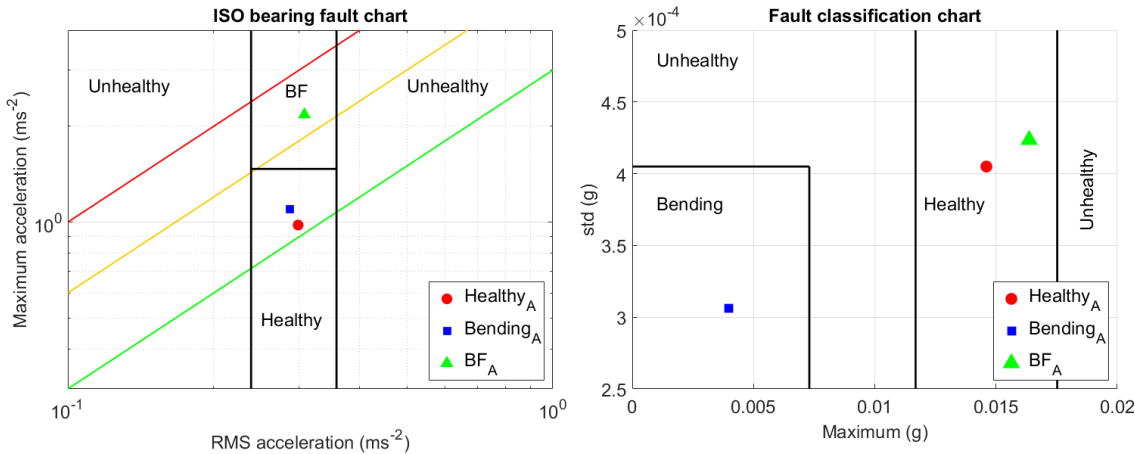


Figure 6.5: Charts showing how condition is diagnosed using time domain (bearing fault severity) and frequency domain (fault classification)

relative to this baseline, based on the tests covered in the previous chapter.

In the time domain, conditions are:

- **Healthy** - $0.8 * RMS_{healthy} < RMS < 1.2 * RMS_{healthy}$ and $max < 1.5 * max_{healthy}$
- **Bearing Fault** - $0.8 * RMS_{healthy} < RMS < 1.2 * RMS_{healthy}$ and $max > 1.5 * max_{healthy}$
- **Unhealthy** - Else

In the frequency domain:

- **Healthy** - $0.8 * max_{healthy} < max < 1.2 * max_{healthy}$
- **Bending** - $max < 0.5 * RMS_{healthy}$ and $std < std_{healthy}$
- **Unhealthy** - Else

These classifications are shown relative to the average values of the samples tested in the previous chapter in Fig 6.5. While the limits are basic, they should prove effective. As the healthy state of the CML is known to change, making decisions relative to a set state allows for proper testing to take place, as opposed to strict numerical limits. Monitoring relative changes has also been found to be a sensible approach for a range of machinery [3].

6.1.4 Communication

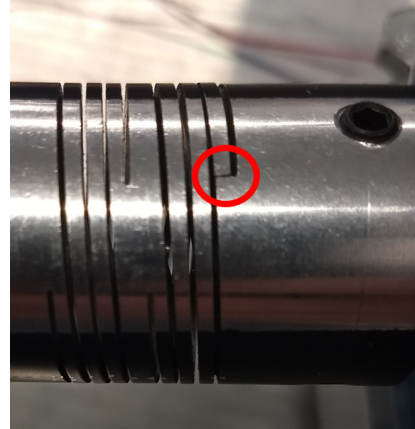
There are many protocols and methods for communication of condition monitoring systems [53]. The embedded CMS uses serial communication combined with NMEA 0183, a popular protocol for GPS units and other devices in the maritime industry [75]. It is a simple protocol, which is also easy to implement, and relevant to the future application of this system. An industrial implementation would have to meet wiring standards for RS232, but for testing the message is sent over a USB cable at low voltage [75]. The data fields and expected values are detailed in Table 6.1. The messages are read and stored on the computer using an NMEA Python library to interpret [76]. A custom class was created for the embedded CMS.

	\$PCBM,...<0D><0A>
Data field	Notes
Identifier	P - Proprietary message format CBM - Sentence Type
Message type	M - MCSA V - Vibration Analysis
Domain	T - Time domain F - Frequency Domain
Hour	Hours since start (0-99)
Minutes	Minutes past hour (0-60)
Max Freq	Frequency with largest component
Maximum	Magnitude of largest value (0-65535)
RMS	RMS of values in domain (0-65535)
Std	Standard deviation of values in domain (0-65535)
Condition	MCSA: R - Running S - Stopped L - Loading up/down U - Unhealthy Vibration analysis: H - Healthy U - Unhealthy B - Bending F - Faulty Bearing
Runtime	Recorded runtime of motor

Table 6.1: Proprietary NMEA message format for ECMS



(a) Pock marks on shaft



(b) Crack on flexible coupling

Figure 6.6: Damage on CML

6.2 Long Term Test

To test the system adequately, it was necessary to run the CML for several hours continuously, varying the condition where possible, while monitoring output from the system. This would demonstrate the ability of the system to run independently and allow evaluation of the system accuracy in diagnosis. Unfortunately, this precludes testing for a bearing fault, as changing a bearing on the CML is an arduous process and it is difficult to ensure that there are no other changes to the CML such as bending or movement. While changing out the bearing during previous testing, damage was also made to the shaft and flexible coupling which could interfere with testing (Fig 6.6). Therefore, the test will induce healthy and bending states only. Once a healthy state is stored, bending can be induced and should have a similar effect to the changes measured previously. The motor will also be run up to and down from its full operating speed, to test the ability of the MCSA to identify the rotor speed.

Results

The output from the embedded CMS is displayed visually in Fig 6.8. The system worked as expected, providing data every minute for four hours and setting new healthy states when requested. MCSA effectiveness in identifying full running speed can be seen by the gaps in data for the vibration time and frequency domains, relative to the current level. Differences between gradual motor run up/down and immediate starts/stops can also be seen on the MCSA chart where the current level is not stable and is identified as loading. In this case, the current threshold proved effective, although in practice the background noise level may be higher and will have to be taken into account. MCSA does not identify unhealthy behaviour in the motor, as expected.

Within the time domain, only healthy and unhealthy conditions are transmitted. This is expected as the faulty bearing was not tested for explicitly. However, using the values from the time domain, the CML actually breaches the alarm limits for each vibration reading which was taken (Fig 6.7). This suggests that there is in fact a significant fault with the CML in its current state. It is possible that one

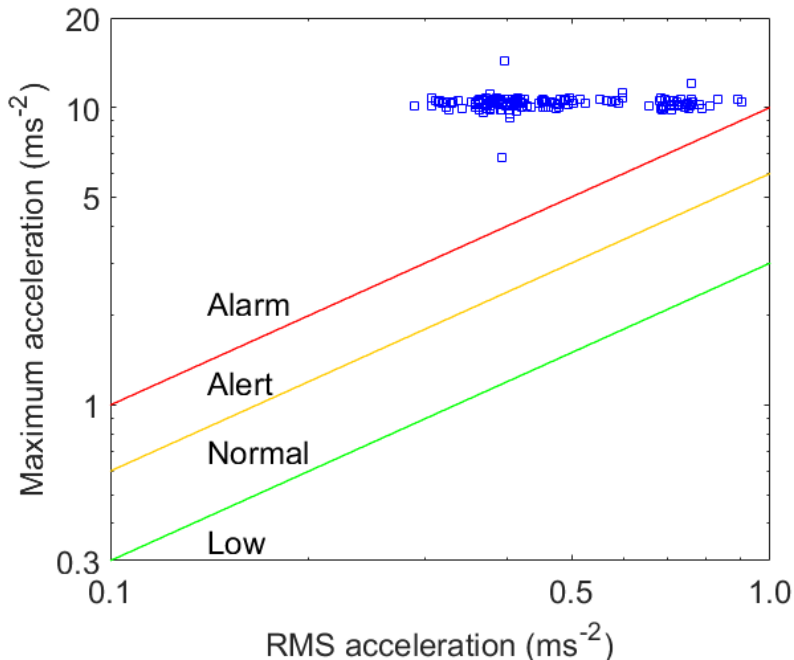


Figure 6.7: Results from long term test time domain compared to ISO bearing fault standard

of the bearings was damaged while preparing the CML for testing. The impulses could also result from the damaged coupling. Future implementations could include numerical limits as a condition indicator. There is significant variation shown for the max values, but when an unhealthy condition is identified it is often due to changes in the RMS value.

The frequency domain, as expected, provides more information about the condition of the CML and is able to identify bending in several instances. At times, bending was misdiagnosed as simply unhealthy. The unhealthy diagnoses often align with unhealthy diagnosis from the time domain. This suggests that faults other than simply bending may be surfacing. Regardless of the exact cause, the system correctly identifies changes in condition. The FFT max varies significantly across time and appears to be the prime indicator of condition.

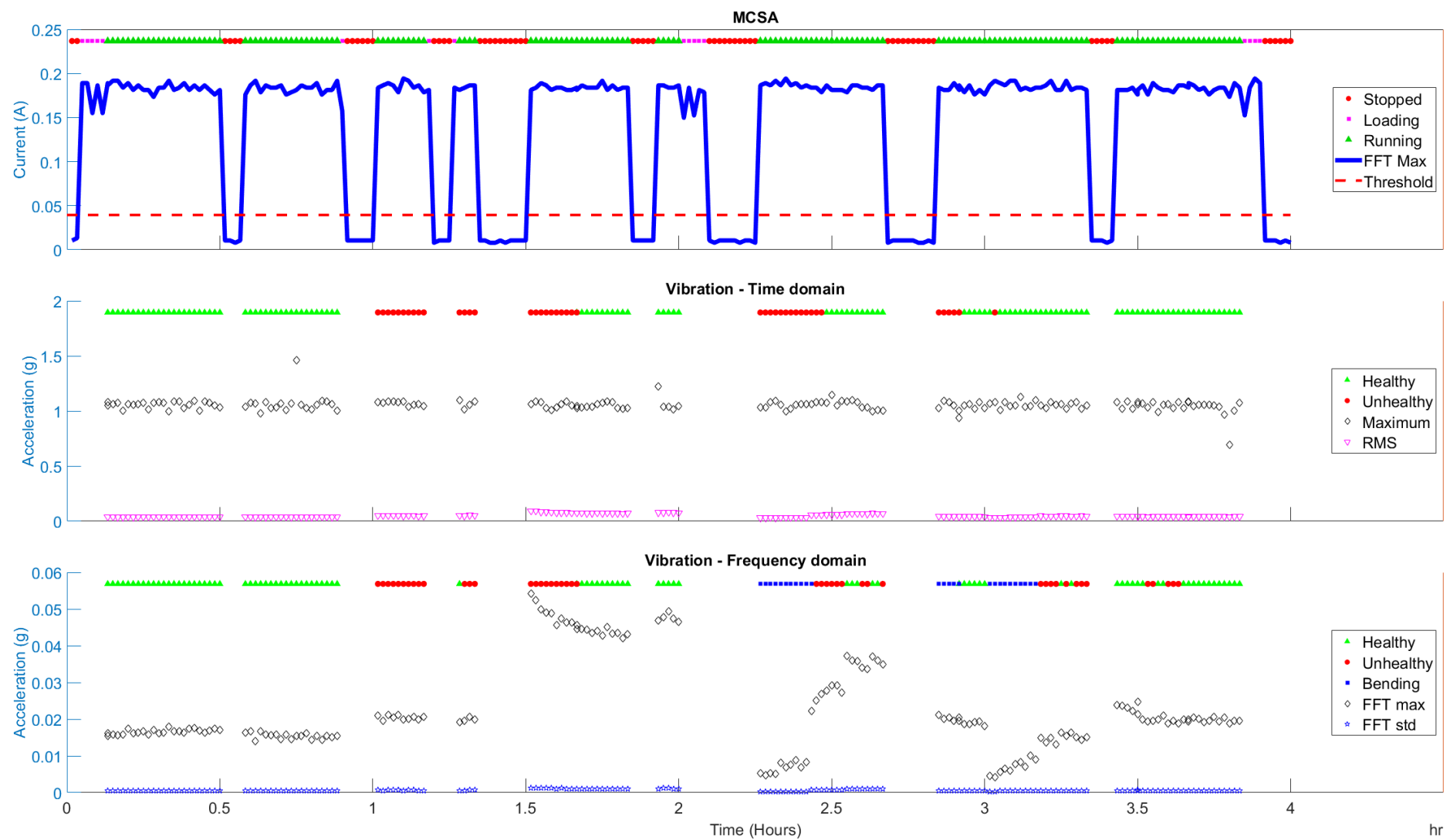


Figure 6.8: Overview of results from long term testing of embedded CMS

Test	Average Power (mW)
Base	7.333
LPM	2.995
Accelerometer Only	8.902
CT Only	64.089
Both Sensors	66.980
Running and LPM	60.438

Table 6.2: Results of power consumption tests

6.3 Power Consumption

To inform further design decisions of the embedded CMS, power consumption of the system was monitored in several states. The MSP432 Launchpad includes hardware specifically for monitoring power consumption as a program runs, through a technology known as EnergyTrace [77]. Energy consumption which travels through an on-board DC-DC converter is closely monitored, allowing even short device activity to be discerned. The EnergyTrace tool in Code Composer Studio 8.1.0.0011 was used for measurements.

Of interest are the effects of using low power mode (LPM) and what the energy cost of the sensors is. The condition parameters were altered so that MCSA and vibration channels would be sampled regardless of their readings, using only the RTC trigger. The board was run, without sensors, for five minutes to ensure that several reads were included in the results. LPM, or ‘sleep’, was then induced in the program between reads. In LPM, no processing can take place. The board waits for the read triggers which ‘wake’ the device [60]. Separately, the default program was run with a CT, a vibration sensor and then both sensors. Finally, a fully operational version of the program with LPM was tested while taking measurements and condition decisions on the condition monitoring rig.

Naturally, adding sensors should increase the power consumption significantly. According to their datasheets: the accelerometer consumes a maximum of 0.4 mA; the CT consumes a maximum of 25 mA [67][71]. The effect of LPM is not as clear as it depends strongly on the structure of the program [60].

Results

A sample of the results which highlights the effect of processing and transmission is shown in Fig 6.9. Many individual features of the program are recognisable. The effects of LPM and the sensors can be seen clearly. It is also clear that if many readings were triggered, the power consumption would increase dramatically.

The average power consumption values suggest that the primary component of power consumption in the system is the CT 6.2. LPM decreases consumption significantly for the full system. The consumption is above what could be expected from an energy harvesting system [52]. Future versions should investigate the possibility of disabling sensors when they are not in use to decrease waste.

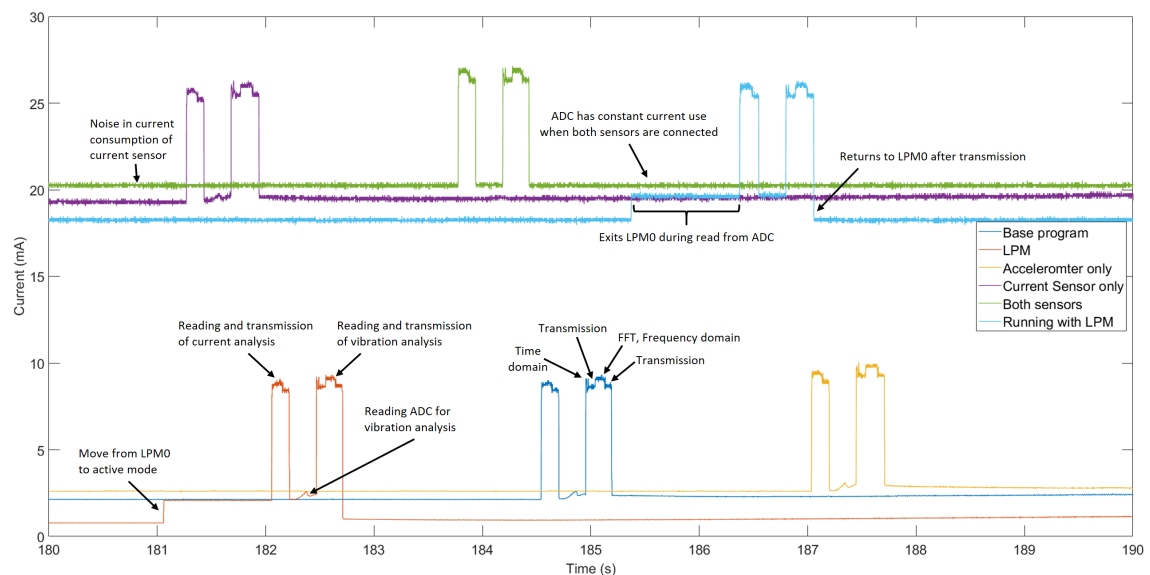


Figure 6.9: Annotated current levels for different system states during reading, processing and transmission of data (signals offset in time for clarity)

Chapter 7

Conclusion and Future Work

An embedded CMS has been designed and implemented, which performs online processing and FDD, transmitting the condition of a motor system and useful statistics for further processing. Low cost hardware and simple signal processing techniques were shown to be sufficient to diagnose a range of faults. The statistics extracted have demonstrated potential to train ANNs, so building a system which can calculate and transmit them paves the way for more intelligent use of this information in real world applications.

The effectiveness of MEMS A highlights that accelerometers should be chosen with properties particular to the application. Despite performing poorly during modular testing, MEMS A was well suited to the CML due to its high sensitivity, high resonant frequency and frequency response characteristics. Overall, vibration analysis was shown to be a good tool for FDD.

Similarly, MCSA still proved valuable as an element of the embedded CMS. Providing very clean data about the supply frequency of the motor guaranteed that vibration analysis took place only at full operating speed. It also measured the runtime of the motor; simple information which would immediately be useful for maintaining marine pumps.

The embedded CMS was shown to operate remotely and communicate using the NMEA protocol. This would significantly improve ease of implementation on board a ship for testing.

7.1 Future Work

FDD and the cloud

Improvements to the embedded CMS presented in this paper include:

- Use in-place FFT to increase the number of samples which can be stored and therefore the resolution of the frequency domain
- More complex MCSA diagnosis techniques such as Park's Vector should be assessed
- Implement order tracking for vibration analysis at different rotor speeds
- Connect the embedded CMS to a cloud solution to store and analyse the data

Condition Monitoring Laboratory

While the CML has provided a testbench for this project, distinct improvements are required to further develop and test CMSs. Presently, it is simply too difficult to ensure a healthy condition will be maintained between tests. The separate elements of the CML should be fixed to prevent movement and misalignment.

There is damage to the shaft, bearing and flexible coupling. These elements should be replaced and the method for swapping bearings, to use a faulty bearing for example, should be made easier.

The system for inducing bending in the shaft needs to be improved. Either recalibration should be performed or the linear actuator could be replaced with a stepper motor.

Acquiring a motor which provides easier access to internal components would allow for testing and diagnosis of electrical faults. This would provide more information about the relative merits of MCSA and vibration analysis.

Preparation for real world application

There are significant changes which need to be made before the embedded CMS could be implemented on a ship. Encasing of the processor board and sensors is essential to prevent damage to these components. Suitable wiring should be used to prevent damage or interference in the signals.

Lloyd's Register have proposed testing on a local ferry. This would be an excellent opportunity to find out how the system performs and what further challenges remain.

Further work will be required to reduce the energy usage of the system and show that it can be powered in a sustainable manner. By switching off sensors when they are not required and using low power modes for as long as possible, power consumption may be reduced to a level where the system can be powered from energy harvesting [52]. This would present a much more realistic proposition for ship operators, builders and pump manufacturers alike.

Bibliography

- [1] F. S. Nowlan and H. F. Heap, *Reliability-centered maintenance*. Dolby Access Press, 1978.
- [2] A. K. Jardine, D. Lin, and D. Banjevic, “A review on machinery diagnostics and prognostics implementing condition-based maintenance,” *Mechanical Systems and Signal Processing*, vol. 20, no. 7, pp. 1483–1510, 2006.
- [3] R. B. Randall, *Vibration-based Condition Monitoring: Industrial, Automotive and Aerospace*. John Wiley & Sons, 2011.
- [4] A. Sundberg, “Management aspects on condition based maintenance – the new opportunity for maritime industry,” *Paper presented at the 9TH International Conference on Marine Engineering Systems at the Helsinki University of Technology*, May 2003.
- [5] I. Lazakis, Y. Raptodimos, and T. Varelas, “Predicting ship machinery system condition through analytical reliability tools and artificial neural networks,” *Ocean Engineering*, vol. 152, p. 404–415, 2018.
- [6] C. Norden, K. Hribernik, Z. Ghrairi, and C. Fuggini, “New approaches to through-life asset management in the maritime industry,” *Through-life Engineering Services Decision Engineering*, p. 423–438, 2014.
- [7] H. Wang, O. L. Osen, G. Li, W. Li, H.-N. Dai, and W. Zeng, “Big data and industrial internet of things for the maritime industry in northwestern norway,” *TENCON 2015 - 2015 IEEE Region 10 Conference*, 2015.
- [8] Z. Hameed, S. Ahn, and Y. Cho, “Practical aspects of a condition monitoring system for a wind turbine with emphasis on its design, system architecture, testing and installation,” *Renewable Energy*, vol. 35, no. 5, p. 879–894, 2010.
- [9] C. Granell, D. Havlik, S. Schade, Z. Sabeur, C. Delaney, J. Pielorz, T. Usländer, P. Mazzetti, K. Schleidt, M. Kobernus, F. Havlik, N. R. Bodsberg, A. Berre, and J. L. Mon, “Future internet technologies for environmental applications,” *Environmental Modelling & Software*, vol. 78, pp. 1 – 15, 2016.
- [10] Lloyd’s Register, “Pump analytics - condition monitoring of a sea water cooling pump,” Personal Communication, 2018.
- [11] Crabtree and Zappala, “Survey of commercially available condition monitoring systems for wind turbines,” *Technical Report, Durham University School of Engineering and Computing Sciences and the SUPERGEN Wind Energy Technologies Consortium*, 2014.

BIBLIOGRAPHY

- [12] M. Sen and B. Kul, "Iot-based wireless induction motor monitoring," *2017 XXVI International Scientific Conference Electronics (ET)*, 2017.
- [13] G. M. K. Knutsen and B. Vartdal, "White paper: Beyond condition monitoring in the maritime industry," DNV GL, Tech. Rep., January 2014. [Online]. Available: <https://www.dnvg.com/news/dnv-gl-beyond-condition-monitoring-in-the-maritime-industry-7685>
- [14] R. Ahmad and S. Kamaruddin, "An overview of time-based and condition-based maintenance in industrial application," *Computers & Industrial Engineering*, vol. 63, no. 1, p. 135–149, 2012.
- [15] A. Salonen and M. Deleryd, "Cost of poor maintenance," *Journal of Quality in Maintenance Engineering*, vol. 17, no. 1, p. 63–73, 2011.
- [16] ISO, "Condition monitoring and diagnostics of machines - General guidelines," International Organization for Standardization, Geneva, CH, Standard, 2018.
- [17] I. Lazakis, Y. Raptodimos, and T. Varelas, "Predicting ship machinery system condition through analytical reliability tools and artificial neural networks," *Ocean Engineering*, vol. 152, p. 404–415, 2018.
- [18] M. Stopford, *Maritime economics*. Routledge, 2010.
- [19] D. Shorten, "Marine machinery condition monitoring," Sep 2012. [Online]. Available: <https://dannyshorten.files.wordpress.com/2012/09/marine-machinery-condition-monitoring-sunderland-2012-final.pdf>
- [20] Lloyd's Register, "Annexes to machinery planned maintenance and condition monitoring," Lloyd's Register, Tech. Rep., May 2017. [Online]. Available: <https://www.cdlive.lr.org/information/documents/ShipRight/Linked%20Supporting%20Services/Machinery%20Planned%20Maintenance%20and%20CM/Machinery%20Planned%20Maintenance%20and%20Condition%20Monitoring,%20Annexes%20May%202017.pdf>
- [21] L. W. T. H. W. H. N. W. E. S. K Esmaeili, M Zuercher, "Advanced signal processing techniques for wind turbine gearbox bearing failure detection," in *First World Congress on Condition Monitoring 2017: Condition monitoring (CM) methods and technologies*, London, United Kingdom, 2017.
- [22] X. Dai and Z. Gao, "From model, signal to knowledge: A data-driven perspective of fault detection and diagnosis," *IEEE Transactions on Industrial Informatics*, vol. 9, no. 4, p. 2226–2238, 2013.
- [23] ISO, "Mechanical vibration - evaluation of machine vibration by measurements on non-rotating parts," International Organization for Standardization, Geneva, CH, Standard, 2009.
- [24] J. Igba, K. Alemzadeh, C. Durugbo, and E. T. Eiriksson, "Analysing rms and peak values of vibration signals for condition monitoring of wind turbine gearboxes," *Renewable Energy*, vol. 91, p. 90–106, 2016.

- [25] ISO, "Conditional monitoring and diagnostics of machines - guidelines for vibration diagnosis," International Organization for Standardization, Geneva, CH, Standard, 2015.
- [26] F. Bonnardot, R. B. Randall, and J. Antoni, "Enhanced unsupervised noise cancellation using angular resampling for planetary bearing fault diagnosis," *The International Journal of Acoustics and Vibration*, vol. 9, no. 2, 2004.
- [27] D. Ho and R. Randall, "Optimisation of bearing diagnostic techniques using simulated and actual bearing fault signals," *Mechanical Systems and Signal Processing*, vol. 14, no. 5, p. 763–788, 2000.
- [28] ISO, "Conditional monitoring and diagnostics of machines - vibration condition monitoring," International Organization for Standardization, Geneva, CH, Standard, 2009.
- [29] C. Crabtree, D. Zappala, and P. Tavner, "Survey of commercially available condition monitoring systems for wind turbines," Durham University School of Engineering and Computing Sciences and the SUPERGEN Wind Energy Technologies Consortium, Tech. Rep., 2014. [Online]. Available: <http://dro.dur.ac.uk/12497/1/12497.pdf?DDD10+ttsd23+dul4eg>
- [30] R. Polikar, "The wavelet tutorial - second edition," Aug 2013. [Online]. Available: <http://web.iitd.ac.in/~sumeet/WaveletTutorial.pdf>
- [31] S. Banerjee, R. Gupta, and M. Mitra, "Delineation of ecg characteristic features using multiresolution wavelet analysis method," *Measurement*, vol. 45, no. 3, p. 474–487, 2012.
- [32] B. Corne, B. Vervisch, C. Debruyne, J. Knockaert, and J. Desmet, "Comparing mcsa with vibration analysis in order to detect bearing faults — a case study," *2015 IEEE International Electric Machines & Drives Conference (IEMDC)*, 2015.
- [33] J. Medina-García, T. Sánchez-Rodríguez, J. Galán, A. Delgado, F. Gómez-Bravo, and R. Jiménez, "A wireless sensor system for real-time monitoring and fault detection of motor arrays," *Sensors*, vol. 17, no. 3, p. 469, 2017.
- [34] R. S. D. Gama, C. C. J. Silva, C. E. F. Nascimento, A. M. D. Silva, and C. D. Costa, "Analysis of combined motor current signature and vibration-monitoring techniques in the study of broken bars in three-phase high-performance induction motors," *Journal of Electrical & Electronic Systems*, vol. 06, no. 03, 2017.
- [35] ISO, "Conditional monitoring and diagnostics of machines - diagnostic techniques for electric motors," International Organization for Standardization, Geneva, CH, Standard, 2017.
- [36] T. H. B. Z. A. W. N. W. I Bashir, L Wang, "Integrated smart bearings for next generation aero-engines part 1: Development of a sensor suite for automatic bearing health monitoring," in *First World Congress on Condition Monitoring 2017: Condition monitoring (CM) methods and technologies*, London, United Kingdom, 2017.

BIBLIOGRAPHY

- [37] B. Dolenc, P. Boškoski, and D. Juričić, “Distributed bearing fault diagnosis based on vibration analysis,” *Mechanical Systems and Signal Processing*, vol. 66-67, p. 521–532, 2016.
- [38] S. Mcinerny and Y. Dai, “Basic vibration signal processing for bearing fault detection,” *IEEE Transactions on Education*, vol. 46, no. 1, p. 149–156, 2003.
- [39] A. Moosavian, M. Khazaee, H. Ahmadi, M. Khazaee, and G. Najafi, “Fault diagnosis and classification of water pump using adaptive neuro-fuzzy inference system based on vibration signals,” *Structural Health Monitoring: An International Journal*, vol. 14, no. 5, p. 402–410, 2015.
- [40] R. Parekh, “An887 - ac induction motor fundamentals,” 2003. [Online]. Available: <http://www.microchip.com/wwwAppNotes/AppNotes.aspx?appnote=en012135>
- [41] ISO, “Condition monitoring and diagnostics of machine systems - electrical signature analysis of three-phase induction motors,” International Organization for Standardization, Geneva, CH, Standard, 2013.
- [42] G. Joksimovic, J. Riger, T. Wolbank, N. Peric, and M. Vasak, “Stator line current spectrum content of a healthy cage rotor induction machine,” *8th IEEE Symposium on Diagnostics for Electrical Machines, Power Electronics & Drives*, 2011.
- [43] W. Thomson and M. Fenger, “Case histories of current signature analysis to detect faults in induction motor drives,” *IEEE International Electric Machines and Drives Conference, 2003. IEMDC03.*, 2003.
- [44] M. E. H. Benbouzid, “A review of induction motors signature analysis as a medium for faults detection,” *IECON 98. Proceedings of the 24th Annual Conference of the IEEE Industrial Electronics Society (Cat. No.98CH36200)*, 1998.
- [45] A. Cardoso, S. Cruz, and D. Fonseca, “Inter-turn stator winding fault diagnosis in three-phase induction motors, by parks vector approach,” *1997 IEEE International Electric Machines and Drives Conference Record*, 1997.
- [46] A. Cardoso, S. Cruz, J. Carvalho, and E. Saraiva, “Rotor cage fault diagnosis in three-phase induction motors, by parks vector approach,” *IAS 95. Conference Record of the 1995 IEEE Industry Applications Conference Thirtieth IAS Annual Meeting*, 1995.
- [47] A. J. M. C. S. M. A. Cruz, “Rotor cage fault diagnosis in three-phase induction motors by extended park’s vector approach,” *Electric Machines & Power Systems*, vol. 28, no. 4, pp. 289–299, 2000.
- [48] J. Lehtinen, J. Munkberg, J. Hasselgren, S. Laine, T. Karras, M. Aittala, and T. Aila, “Noise2Noise: Learning image restoration without clean data,” in *Proceedings of the 35th International Conference on Machine Learning*, ser. Proceedings of Machine Learning Research, J. Dy and A. Krause, Eds., vol. 80. Stockholm, Sweden: PMLR, 10–15 Jul 2018, pp. 2965–2974.

- [49] A. C. Lima-Filho, R. D. Gomes, M. O. Adissi, T. A. B. D. Silva, F. A. Belo, and M. A. Spohn, “Embedded system integrated into a wireless sensor network for online dynamic torque and efficiency monitoring in induction motors,” *IEEE/ASME Transactions on Mechatronics*, vol. 17, no. 3, p. 404–414, 2012.
- [50] G. M. Lozito, M. Schmid, S. Conforto, F. R. Fulginei, and D. Bibbo, “A neural network embedded system for real-time estimation of muscle forces,” *Procedia Computer Science*, vol. 51, p. 60–69, 2015.
- [51] Z.-K. Zhang, M. C. Y. Cho, C.-W. Wang, C.-W. Hsu, C.-K. Chen, and S. Shieh, “Iot security: Ongoing challenges and research opportunities,” *2014 IEEE 7th International Conference on Service-Oriented Computing and Applications*, 2014.
- [52] K. Farinholt, N. Brown, J. Siegel, J. Mcquown, and R. Humphris, “Energy harvesting to power embedded condition monitoring hardware,” *Industrial and Commercial Applications of Smart Structures Technologies 2015*, Jan 2015.
- [53] W. Staszewski, A. Jabłoński, and K. Dziedziech, “A survey of communication protocols in modern embedded condition monitoring systems,” *Diagnostyka*, vol. 19, no. 2, p. 53–62, 2018.
- [54] A. Albarbar, S. Mekid, A. Starr, and R. Pietruszkiewicz, “Suitability of mems accelerometers for condition monitoring: An experimental study,” *Sensors*, vol. 8, no. 2, p. 784–799, Jun 2008.
- [55] A. Albarbar, A. Badri, J. K. Sinha, and A. Starr, “Performance evaluation of mems accelerometers,” *Measurement*, vol. 42, no. 5, p. 790–795, 2009.
- [56] P. Ripka, “Electric current sensors: a review,” *Measurement Science and Technology*, vol. 21, no. 11, p. 112001, 2010.
- [57] *Remote Access Laboratory: Vibration Monitoring Demonstrator*, University of Southampton, 2014.
- [58] ABB, “Abb m2va induction motor datasheet.” [Online]. Available: <https://new.abb.com/products/ABB3GVA062002-BSA>
- [59] Omega Engineering, “Industrial accelerometers.” [Online]. Available: <https://www.omega.com/pptst/ACC786A.html>
- [60] Texas Instruments, “Msp432p401r simplelink microcontroller launchpad™ developement kit (msp-exp432p401r),” Texas Instruments, User’s Guide, 2018.
- [61] ——, “Msp430 iqmathlib users guide version,” Texas Instruments, Tech. Rep., 2015. [Online]. Available: <http://www.ti.com/lit/ug/sprugg9/sprugg9.pdf>
- [62] Tran-Thong and B. Liu, “Fixed-point fast fourier transform error analysis,” *IEEE Transactions on Acoustics, Speech, and Signal Processing*, vol. 24, no. 6, p. 563–573, 1976.
- [63] W.-H. Chang and T. Nguyen, “On the fixed-point accuracy analysis of fft algorithms,” *IEEE Transactions on Signal Processing*, vol. 56, no. 10, p. 4673–4682, 2008.

BIBLIOGRAPHY

- [64] M. Borgerding, *Kiss FFT*, Jun 2013. [Online]. Available: <https://sourceforge.net/projects/kissfft/>
- [65] A. Ltd, “Complex fft functions,” Feb 2018. [Online]. Available: http://www.keil.com/pack/doc/CMSIS/DSP/html/group__ComplexFFT.html
- [66] Texas Instruments, “Msp432p401r, msp432p401m simplelink™ mixed-signal microcontrollers,” Texas Instruments, Tech. Rep., 2017.
- [67] Freescale Semiconductor, *MMA7361L*, Apr 2008, rev. 0. [Online]. Available: https://www.nxp.com/files-static/sensors/doc/data_sheet/MMA7361L.pdf
- [68] Analog Devices, *ADXL354/ADXL355*, Apr 2018, rev. 0. [Online]. Available: http://www.analog.com/media/en/technical-documentation/data-sheets/ADXL354_355.pdf
- [69] ——, *ADXL1001/ADXL1002*, Mar 2017, rev. 0. [Online]. Available: <http://www.analog.com/media/en/technical-documentation/data-sheets/adxl1001-1002.pdf>
- [70] Frederiksen, *Instruction Manual for the Vibration Generator no. 2185.00*, Jul 2014, rev. 0.
- [71] LEM, *Current Transducer HO-P/SP33 Series*, Oct 2014, version 2. [Online]. Available: <https://docs-emea.rs-online.com/webdocs/15c5/0900766b815c552c.pdf>
- [72] ——, *Current Transducer HO-P Series*, July 2015, version 5. [Online]. Available: <https://docs-emea.rs-online.com/webdocs/15c5/0900766b815c552d.pdf>
- [73] S. W. Laboratory, *Certificate A.C Ammeter Model S.81 No.AL33433*, Feb 1959.
- [74] BSI, “Elastomer insulated fire resistant (limited circuit integrity) cables for fixed wiring in ships and on mobile and fixed offshore units,” British Standards Institution, London, UK, Standard, 1999.
- [75] D. DePriest, “Nmea data.” [Online]. Available: <http://www.gpsinformation.org/dale/nmea.htm>
- [76] T. Flanagan, “Pynmea2.” [Online]. Available: <https://github.com/Knio/pynmea2>
- [77] Texas Instruments, “Msp430 advanced power optimizations: Ulp advisor™ software and energytrace™ technology,” Jun 2014. [Online]. Available: <http://www.ti.com/lit/an/slaa603/slaa603.pdf>